



Development of a 10-year (2001–2010) 0.1° data set of land-surface energy balance for mainland China

X. Chen¹, Z. Su¹, Y. Ma², S. Liu³, Q. Yu⁴, and Z. Xu³

¹Faculty of Geo-Information Science and Earth Observation, University of Twente, Enschede, the Netherlands

²Key Laboratory of Tibetan Environment Changes and Land Surface Processes, Institute of Tibetan Plateau Research, Chinese Academy of Sciences, CAS Center for Excellence and Innovation in Tibetan Plateau Earth Sciences, Beijing, China

³State Key Laboratory of Remote Sensing Science, School of Geography, Beijing Normal University, Beijing, China

⁴Plant Functional Biology & Climate Change Cluster, University of Technology, Sydney, PO Box 123, Broadway, NSW 2007, Australia

Correspondence to: X. Chen (x.chen@utwente.nl)

Received: 20 February 2014 – Published in Atmos. Chem. Phys. Discuss.: 5 June 2014

Revised: 15 September 2014 – Accepted: 17 October 2014 – Published: 10 December 2014

Abstract. In the absence of high-resolution estimates of the components of surface energy balance for China, we developed an algorithm based on the surface energy balance system (SEBS) to generate a data set of land-surface energy and water fluxes on a monthly timescale from 2001 to 2010 at a $0.1 \times 0.1^\circ$ spatial resolution by using multi-satellite and meteorological forcing data. A remote-sensing-based method was developed to estimate canopy height, which was used to calculate roughness length and flux dynamics. The land-surface flux data set was validated against “ground-truth” observations from 11 flux tower stations in China. The estimated fluxes correlate well with the stations’ measurements for different vegetation types and climatic conditions (average bias = 11.2 Wm^{-2} , RMSE = 22.7 Wm^{-2}). The quality of the data product was also assessed against the GLDAS data set. The results show that our method is efficient for producing a high-resolution data set of surface energy flux for the Chinese landmass from satellite data. The validation results demonstrate that more accurate downward long-wave radiation data sets are needed to be able to estimate turbulent fluxes and evapotranspiration accurately when using the surface energy balance model. Trend analysis of land-surface radiation and energy exchange fluxes revealed that the Tibetan Plateau has undergone relatively stronger climatic change than other parts of China during the last 10 years. The capability of the data set to provide spatial and temporal information on water-cycle and land–atmosphere interactions for the Chinese landmass is examined. The product is free to

download for studies of the water cycle and environmental change in China.

1 Introduction

As China is one of the fastest growing and urbanizing economies in the world, changes in land cover and land use can significantly influence the environment by altering land–atmosphere energy and water exchanges (Suh and Lee, 2004; Lin et al., 2009). For instance, rapid urban expansion has substantially changed land-surface heat fluxes in the Pearl River delta (PRD) (Lin et al., 2009), and has increased sensible heat fluxes in the Beijing metropolitan area (C. Zhang et al., 2009). The variability of surface energy balance and its partitioning may also have an important impact on climate variability in China (Sun and Wu, 2001). Similarly, changes in surface energy fluxes have been shown to alter the intensity of the East Asian monsoon (Zhou and Huang, 2008; Qiu, 2013; Hsu and Liu, 2003). In short, understanding variation in energy fluxes is important for the study of climate change in China (Brauman et al., 2007). Nevertheless, the spatial and temporal variability of China’s land-surface energy balance, and the magnitude of each, are still unknown.

While it is of critical importance to understand the partitioning of water and energy distribution across China’s terrestrial surface, accurate monitoring of its spatial and temporal variation is notoriously difficult (Ma et al., 2011). Several

field experiments are being carried out to monitor turbulent fluxes over selected land cover in China by using ground-based eddy covariance devices (Wang et al., 2010; Yu et al., 2006; Y. Ma et al., 2008; Li et al., 2009). However, these measurements are only representative of small areas around the locations where the measurements are being made. For this reason, the establishment of an eddy-covariance flux network cannot provide a complete land-surface heat flux picture for the entire Chinese landmass.

A number of methods can be used to derive land-surface energy fluxes. Jung et al. (2009), for example, generated global spatial flux fields by using a network upscaling method. However, their flux network included only a limited number of flux stations in China. The Global Soil Wetness Project 2 (GSWP-2) (Dirmeyer et al., 2006) produced a global land-surface product on a $1 \times 1^\circ$ grid for the period 1986 to 1995. The Global Land Data Assimilation System (GLDAS) (Rodell et al., 2004) can provide a global coverage in the form of 3-hourly, 0.25° data. Furthermore, products from the European Centre for Medium-Range Weather Forecasts (ECMWF) interim reanalysis (ERA-Interim) (Dee et al., 2011), the National Centers for Environmental Prediction (NCEP) (Kalnay et al., 1996), Modern-Era Retrospective Analysis for Research and Applications (MERRA) (Rienecker et al., 2011) and other reanalysis data can also provide temporally continuous – but coarse – spatial resolution data sets of land-surface fluxes. Jiménez et al. (2011) made an inter-comparison of different land-surface heat flux products. When these products were applied on continental scales, the different approaches resulted in large differences (Vinukollu et al., 2011a; Jiménez et al., 2011; Mueller et al., 2011).

The problems met by using currently available flux data in climate studies of China have been reported by Zhou and Huang (2010). Zhu et al. (2012) have also reported that summer sensible heat fluxes derived from eight data sets (including NCEP, ERA, and GLDAS) of China's Tibetan Plateau region differ from each other in their spatial distribution. In addition, all the flux data sets mentioned above are based on model simulations, which have deficiencies in studying changes in water-cycle and land–air interactions in China (Y. Chen et al., 2013; Su et al., 2013; Wang and Zeng, 2012; L. Ma et al., 2008).

A spatially and temporally explicit estimate of surface energy fluxes is of considerable interest for hydrological assessments and meteorological and climatological investigations (Norman et al., 2003). Satellite-sensed data of surface variables can be used to produce maps of heat and water fluxes on different scales (Wang and Liang, 2008; X. Li et al., 2012; Liu et al., 2010; Vinukollu et al., 2011b). Remote sensing approaches to estimating surface heat and water fluxes have been largely used on regional scales (Fan et al., 2007; Ma et al., 2011; Jia et al., 2012; X. Zhang et al., 2009; Z. Li et al., 2012; Shu et al., 2011), but there is no analysis of satellite-derived data currently underway to produce a complete, physically consistent, decadal land-surface

heat flux data set (Jiménez et al., 2009) for the Chinese landmass. The use of remotely sensed data offers the potential for acquiring observations of variables such as albedo, land-surface temperature, and normalized difference vegetation index (NDVI) on a continental scale for China. Is it possible to use all available satellite-observed land-surface variables directly to calculate high-resolution land-surface fluxes for the Chinese landmass, due to the reanalysis data having a coarse spatial resolution and containing large uncertainty? Since surface fluxes cannot be detected directly by satellite-borne sensors, an alternative for estimating continental water and energy fluxes can be derived by applying the aerodynamic theory of turbulent flux transfer (Ma et al., 2011) or by establishing statistical relationships between related satellite observations and land-surface fluxes (Jiménez et al., 2009; Wang et al., 2007). Most remotely sensed latent heat flux or evapotranspiration products have null values in urban, water, snow, barren and desert areas (Mu et al., 2007; Wang et al., 2007; Jiménez et al., 2009). This is due to the lack of a uniform representation of turbulent exchange processes over different types of land cover in their method. Meanwhile, the aerodynamic turbulent transfer method can describe the flux exchange through changes in surface roughness length over different land covers. Statistical methods establish relationships between satellite-sensed observations (e.g., NDVI, LST, albedo) and land-surface fluxes through various fitting techniques (Wang et al., 2007). The simple relationships established cannot give a reasonable approximation for extreme conditions such as bare soil or other types of non-canopy land cover (e.g., lakes, deserts), because land covers behave significantly differently in land-surface energy flux partitioning. Fortunately, turbulent flux transfer parameterization can overcome the shortcomings of statistical methods and produce spatially continuous distributions of land-surface energy fluxes with prepared meteorological forcing data. For this reason, we chose a more physically based method – turbulent flux parameterization – to produce the data set.

The challenge in using turbulent flux parameterization lies in the transition from regional to continental and global scales, because meteorological data of high resolution (i.e., 1–10 km) are not easily obtained for a large region. Recently, Chinese scientists produced high-resolution meteorological forcing data that can be used in our study. Another issue is the complexity met by the method when combining different spatial and temporal sampling input variables. This is discussed in detail in Sect. 3.1. The last difficulty that has surrounded the application of turbulent flux parameterization on continental scales is the acquisition of roughness length. To address this difficulty, we have developed a remote-sensing-based mixing technique to estimate canopy heights on a continental scale, and use the resulting canopy height data set to derive, for the very first time, the dynamic variation of surface roughness length for the Chinese landmass.

Complex topography (shown by Fig. 1) and climatic conditions in China make it very difficult to obtain a clear picture of the distribution of energy and water fluxes with a high spatial resolution over a relatively long period for such a large area. In our study, we estimate land-surface heat fluxes with energy balance and aerodynamic parameterization formulas in a revised model of the surface energy balance system (SEBS) (Chen et al., 2013b; Chen et al., 2013a; Su, 2002; Timmermans, 2011); previous tests show that the revised model delivers better performance and improvements in cases where the type of land cover in China is bare soil, short canopy or snow (Chen et al., 2013a, b). Sensible heat flux in SEBS was derived from the difference between surface temperature and air temperature by using Monin–Obukhov similarity theory and bulk atmospheric boundary layer similarity (Brutsaert, 1999), which parameterizes ground surface momentum and heat-transfer coefficient maps to take into account surface roughness, canopy height, vegetation cover, and meteorological stability (Su et al., 2001; Su, 2002; Chen et al., 2013b). The latent heat flux can then be estimated from an energy balance model, assuming that surface net radiation and ground flux are known (Ma et al., 2002; Allen et al., 2011; Vinukollu et al., 2011b). We used high-resolution reanalysis meteorological data, which merge model outputs, remote sensing observations, and in situ measurements. In addition, we also assessed the accuracy of the surface energy balance terms (net radiation, sensible heat, latent heat, and ground heat fluxes) and their climatic trends in the preceding decade (2001–2010).

After defining the equations of the SEBS model (Sect. 2), we describe (in Sect. 3) the input data and ground-truth measurements used in the study. Furthermore, we assess the capacity of the remote-sensing-based product to reproduce the range and variability of measured fluxes, by comparing them with in situ flux tower measurements, followed by trend analysis of the spatial patterns of the fluxes (Sect. 4). Concluding remarks are found in Sect. 5.

2 Model description and development

The surface energy balance system model known as SEBS (Su, 2002) uses aerodynamic resistance to create a spatially coherent estimate of land-surface heat fluxes. Some model inputs can be obtained from remote sensing data, while others can be obtained from meteorological forcing data (e.g., GLDAS, ERA and NCEP reanalysis data). The model's equations and the required forcing variables are described in the remainder of this section.

The surface energy balance equation can be expressed as

$$\text{Rn} = G_0 + H + \text{LE}, \quad (1)$$

where Rn is the net radiation flux; G_0 is the ground heat flux, which is parameterized by its relationship with Rn (Su et al.,

2001); H is the sensible heat flux; and LE is the latent heat flux.

LE is computed by using the evaporative fraction after deriving the other three variables in Eq. (1) and taking into consideration energy and water limits (Su, 2002). As these fluxes were produced with a monthly average temporal resolution, energy storage in vegetation is not considered.

Net radiation flux is

$$\text{Rn} = (1 - \alpha) \times \text{SWD} + \text{LWD} - \text{LWU}, \quad (2)$$

where α is broadband albedo, SWD is downward surface short-wave radiation, and LWD and LWU are downward and upward surface long-wave radiation, respectively.

Here, satellite-observed albedo is used. LWU is derived from land-surface temperature (LST) using the Stefan–Boltzmann law. Land-surface emissivity is derived as described in Chen et al. (2013a). LWD and SWD values are obtained from meteorological forcing data.

Sensible heat flux (H) is computed according to the Monin–Obukhov similarity theory (MOST):

$$H = k u_* \rho C_p (\theta_0 - \theta_a) \left[\ln \left(\frac{z-d}{z_{0h}} \right) - \Psi_h \left(\frac{z-d}{L} \right) + \Psi_h \left(\frac{z_{0h}}{L} \right) \right]^{-1}, \quad (3)$$

where k is the von Karman constant; u_* is friction velocity; ρ is air density; C_p is specific heat for moist air; θ_0 is the potential temperature at the ground surface; θ_a is the potential air temperature at height z ; d is the zero plane displacement height; Ψ_h is the stability correction function for sensible heat transfer (Brutsaert, 1999); and L is the Obukhov length. In our study, θ_a was obtained from meteorological forcing data, and θ_0 was derived from Moderate Resolution Imaging Spectroradiometer (MODIS) LST data. For more detailed information about u_* and the calculation of L , see Su (2002) and Chen et al. (2013b).

The roughness height for heat transfer (z_{0h}) in Eq. (3) is calculated as follows:

$$z_{0h} = \frac{z_{0m}}{\exp(kB^{-1})}. \quad (4)$$

Using the fractional canopy coverage kB^{-1} at each pixel can be derived according to the following modification of the equation described by Su et al. (2001):

$$kB^{-1} = f_c^2 \times kB_c^{-1} + f_s^2 \times kB_s^{-1} + 2 \times f_c \times f_s \times kB_m^{-1}, \quad (5)$$

where f_c is fractional canopy coverage and f_s is the fraction of bare soil in one pixel; kB_c^{-1} is the kB^{-1} of the canopy; kB_s^{-1} is the kB^{-1} of bare soil; and kB_m^{-1} is kB^{-1} for mixed bare soil and canopy. As kB^{-1} is the most important parameter in a MOST-based calculation of sensible heat flux, kB^{-1} has been updated by Chen et al. (2013b). The momentum roughness length used to calculate kB_s^{-1} was given a value

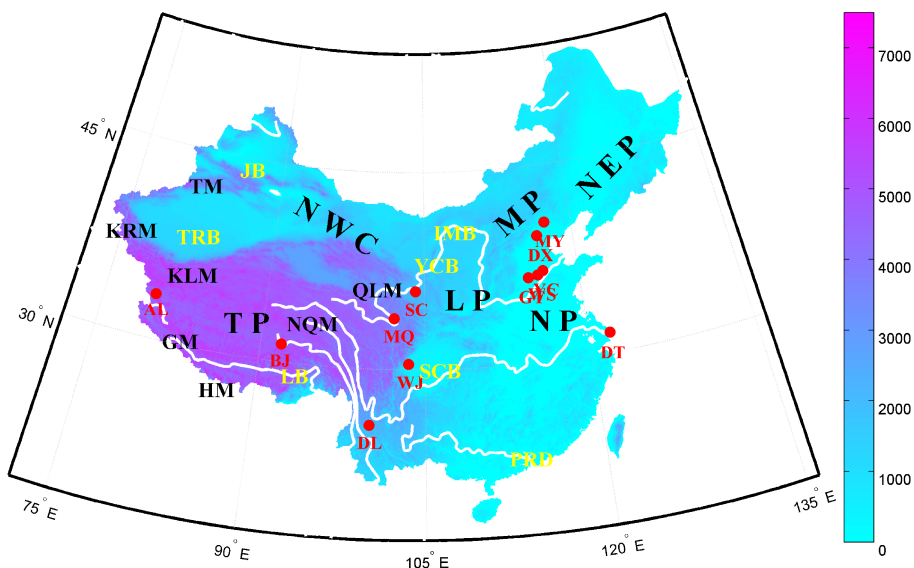


Figure 1. A DEM map (digital elevation map) of the Chinese landmass. The symbols indicate major physical phenomena: Tibetan Plateau (TP), northwestern China (NWC), inner Mongolian Plateau (MP), Loess Plateau (LP), North China Plain (NP), northeastern China Plain (NEP); Pearl River delta (PRD), Sichuan (SCB), Yinchuan (YCB), inner Mongolian (IMB), Lhasa (LB), Tarim (TRB), and Junggar (JB) basins; the Himalaya (HM), Ganges (GM), Kunlun (KL), Karakorum (KRM), Tianshan (TM), Nyainqentanglha (NQM) and Qilian (QLM) mountain ranges. The plateau and plain letter symbols are in black type. The basin letter symbols are in yellow type. The flux station letter symbols are in red type. White lines show several of the major rivers in China. The unit of the color bar is m.

of 0.004 (Chen et al., 2013b), and the heat roughness length of bare soil was calculated according to Yang et al. (2002). The new kB^{-1} gives a better performance than the previous version of kB^{-1} (Chen et al., 2013a, b). Detailed evaluations of the new parameterization of kB^{-1} can be found in Chen et al. (2013b).

The roughness height for momentum transfer z_{om} in Eq. (4) is derived from canopy height (HC), leaf area index (LAI) and the canopy momentum transfer model (Massman, 1997):

$$z_{om} = HC \times (1 - d/HC) \times \exp(-k \times \beta), \quad (6)$$

$$\beta = C_1 - C_2 \times \exp(-C_3 \times C_d \times LAI), \quad (7)$$

where $C_1 = 0.32$, $C_2 = 0.26$, and $C_3 = 15.1$ are model constants related to the bulk surface drag coefficient (Massman, 1997). The three constants have been tested for several canopies (Chen et al., 2013b; Cammalleri et al., 2010) and evaluated as one of the best solutions for canopy turbulent-flux parameterization (Cammalleri et al., 2010). C_d is the drag coefficient, which typically equals 0.2 (Goudriaan, 1977); d is displacement height, which is derived from HC and the wind speed extinction coefficient (Su, 2002; Su et al., 2001).

As Chen et al. (2013b) have pointed out, HC is vital for turbulent heat simulations, which makes accurate estimation of HC for the Chinese landmass important for this study. A remote-sensing-based canopy height method (Chen et al., 2013b) was developed further to estimate

canopy height distribution for the whole of China in this study. Simard et al. (2011) produced a global forest canopy-height map using data from the Geoscience Laser Altimeter System (GLAS) aboard ICESat (Ice, Cloud, and land Elevation Satellite). However, short-canopy (e.g., savanna, crop, grass, and shrub) height information cannot be acquired by laser techniques. Since short-canopy height usually varies by season throughout the year – crops are planted in spring and harvested in autumn – we calculated short-canopy height using an enhancement of the NDVI-based equation from Chen et al. (2013b):

$$HC(LCT) = HC_{\min}(LCT) + \frac{HC_{\max}(LCT) - HC_{\min}(LCT)}{(NDVI_{\max}(LCT) - NDVI_{\min}(LCT))} \times (NDVI(LCT) - NDVI_{\min}(LCT)), \quad (8)$$

where $HC_{\max}(LCT)$ and $HC_{\min}(LCT)$ are the maximum and minimum short-canopy heights for a specific land cover type (LCT); $HC_{\min}(LCT)$ is set to 0.002 m (Chen et al., 2013b); and HC_{\max} is set to 5, 2.5, 0.5, 0.5, and 0.5 m for savannas (including woody savannas), cropland, grassland, shrubland, and barren and sparsely vegetated pixels, respectively. MCD12C1 land cover type 1 in the year of 2002 is used to classify the pixels into savannas, cropland, grassland, and shrubland, barren and sparsely vegetated. $NDVI_{\min}$ and $NDVI_{\max}$ are minimum and maximum NDVI values during our 10-year study period. Each short-canopy pixel was

given an $NDVI_{min}$ and $NDVI_{max}$ value to calculate the short-canopy height.

The NDVI-based short-canopy height method above was used to fill cropland, grassland, shrubland, and barren pixels. The forest canopy heights (greater than 10 m) were assumed to be constant, i.e., with no seasonal change. By merging the forest canopy heights greater than 10 m and the variable short-canopy data, we constructed dynamic monthly maps of canopy heights for the Chinese landmass for the period of 2001–2010. These maps were then used to calculate heat fluxes. Figure 3 gives an example of derived canopy height at 11 Chinese flux stations.

3 Data and validation

Our modeling approach makes use of a variety of satellite-based sensor data and meteorological forcing data to estimate monthly energy and water fluxes across China. The forcing data can come from satellite-based or reanalysis data sets. Due to the influence of weather, satellite-sensed visible and thermal band data (e.g., NDVI, albedo, LST) often have spatial and temporal gaps in daily data. Various temporal and spatial gap-filling algorithms have been developed to produce continuous monthly data for satellite-sensed variables (Chen et al., 2004; Moody et al., 2005). In order to avoid both spatial and temporal gaps in the final product, we selected some specific satellite-sensed data sets for this study (see Table 1). Detailed information about each input variable is described in the following subsections.

The longest period covered by the forcing data set is approximately 31 years; the shortest is about 10 years. The spatial resolution of the data set varies from 0.01 to 0.25° , and its sample frequency from 3 h to 1 month. The meteorological forcing data developed by the Institute of Tibetan Plateau Research, Chinese Academy of Sciences (hereafter referred to as ITPCAS forcing data) (He, 2010), were constructed to study meteorological variation in China. ITPCAS forcing data cover the entire landmass of China, and have the highest temporal resolution among the input data sets used. Other variables such as LST and albedo, for example, have coarser temporal resolutions (monthly) and global coverage. When combining data of different spatial and temporal resolutions, both spatial and temporal scaling issues need to be addressed.

Estimates of land-surface energy flux can be subject to large errors, due to bias in the meteorological forcing input data. The spatial distribution of meteorological variables is closely related to topography (Li et al., 2013). When interpolating meteorological input variables to finer scales, these effects have to be accounted for (Sheffield et al., 2006), which goes beyond the scope of our study. Therefore, we chose to resample the satellite product of a high spatial resolution to a lower spatial resolution that matches the resolution of the meteorological input data. Also, the meteorological data

were averaged to monthly values that have the same temporal resolution as the remotely sensed input variables. ITPCAS forcing data provide us data of the highest spatial resolution among the meteorological forcing data currently available (e.g., ERA-Interim, NCEP, GLDAS, MERRA). Taking into account all these items, our aim was to produce a monthly product of $0.1 \times 0.1^\circ$ resolution land-surface heat fluxes that contains neither spatial nor temporal gaps and that can be used to study seasonal and inter-annual variability in the hydrological and energy cycles of China.

3.1 Input data sets and their validations

3.1.1 Meteorological forcing data

In studies previous to ours, reanalysis data have been applied in many different ways, for example to construct land-surface forcing data (Sheffield et al., 2006), to detect climate trends (Taniguchi and Koike, 2008), and to investigate water and energy cycles on regional and continental scales (Roads and Betts, 2000). Reanalysis data have also been applied by the remote sensing community to derive estimates of global terrestrial evapotranspiration and gross primary production (Mu et al., 2007; Yuan et al., 2010). Few studies, however, have used reanalysis data together with remotely sensed ground data to derive global land-energy fluxes (sensible heat flux, latent heat flux, net radiation, etc.).

Researchers have developed several kinds of reanalysis data. Comparisons and evaluations of these reanalysis products with in situ observations have been performed for individual sites, specific regions, and the entire globe (Wang and Zeng, 2012; Decker et al., 2011). It is well known that inaccuracies existing in reanalysis forcing data may have substantial impacts on the simulation of land-surface energy partitioning. It is difficult to choose which reanalysis data are better for use as forcing data. Additionally, the spatial resolution of all of the above reanalysis/forcing data sets is not as high as that of remote sensing data. The ITPCAS forcing data set was produced by merging a variety of data sources. This data set benefits in particular from the merging of information from 740 weather stations operated by the China Meteorological Administration that have not been used in other forcing data. The data set has already been used to run land-surface models, and has been shown to be more accurate than other forcing data sets (Chen et al., 2011; Liu and Xie, 2013). ITPCAS meteorological forcing data include variables such as instantaneous near-surface air temperature (T_a), near-surface air pressure (P), near-surface air-specific humidity (Q), near-surface wind speed (W_s) at a temporal resolution of 3 h, and 3-hourly mean downward surface short-wave (SWD) and downward surface long-wave (LWD) radiation. The time period covered is from 1979 to 2010; the spatial resolution has a grid size of $0.1 \times 0.1^\circ$.

Table 1. Input data sets used for calculating land-surface fluxes for China (see Sects. 2 and 3 for an explanation of abbreviations).

Variables	Data source	Temporal resolution	Availability	Domain	Spatial resolution (degrees)	Method
SWD	ITPCAS	3 h	1979–2010	China land	0.1	Reanalysis
SWU	ITPCAS & GlobAlbedo	3 h	2000–2010	China land	0.1	Satellite and reanalysis
LWD	ITPCAS	3 h	1979–2010	China land	0.1	Reanalysis
LWU	MOD11C3 & MYD11C3 V5 & Emis of Chen et al. (2013b)	1 month	2000–2012	China land	0.05	Satellite
T_a	ITPCAS	3 h	1979–2010	China land	0.1	Reanalysis
Q	ITPCAS	3 h	1979–2010	China land	0.1	Reanalysis
W_s	ITPCAS	3 h	1979–2010	China land	0.1	Reanalysis
P	ITPCAS	3 h	1979–2010	China land	0.1	Reanalysis
LST	MOD11C3 V5 & MYD11C3 V5	1 month	2000–2012	Global	0.05	Satellite
h_c	GLAS & SPOT VEGETATION	1 month	2000–2012	China land	0.01	Satellite
α	GlobAlbedo	1 month	2000–2010	Global	0.05	Satellite
NDVI	SPOT VEGETATION	10 days	1998–2012	Global	0.01	Satellite
LAI	MOD15A2 & MCD15A2	8 days	Feb 2000–Jul 2002; Aug 2002–2012	Global	0.01	Satellite
Land cover	MCD12C1	Yearly	2002	Global	0.05	Satellite

3.1.2 MODIS land-surface temperature processing

MODIS (MODerate-resolution Imaging Spectroradiometer) sensors have been used to produce several global- and continental-scale LST data sets. MOD11C3 V5 and MYD11C3 V5 products (Wan, 2009) are validated over a range of representative conditions, with an average bias of less than 1 K (Coll et al., 2009; Wan and Li, 2008). The MODIS V5 monthly LST product, MOD11C3 and MYD11C3, has a 0.05° grid size, without gaps, and covers the period March 2000 to the near-present. It provides monthly daytime and night-time LST values. In our study, we averaged the daytime and night-time values of MOD11C3 and MYD11C3 to represent monthly means.

After spatially interpolating the monthly mean LST from $0.05 \times 0.05^\circ$ to $0.1 \times 0.1^\circ$ resolution, we picked out LST values of pixels that included the 11 flux tower stations from which in situ measurements were gathered. The time series comparisons of LST with the ground measurements were shown by Fig. 2. It shows that the processed monthly LST can present the seasonal variations in LST over different land covers very well. The pixel values were validated against the in situ LST measurements. Detailed information about each station is given in Sect. 3.2. The linear correlation ($R = 1.0$), RMSE ($= 1.9$ K) and MB (mean value of the satellite data minus in situ observation equals 0.5 K) indicate that the quality of the merged remotely sensed monthly LST data in China is high. They also show that the monthly LST captures the in situ LST variability of different elevations and land surfaces, which described in Sect. 4.2.

3.1.3 Albedo

Land-surface albedo determines the fraction of short-wave radiation absorbed by the ground, thus influencing the surface energy budget. Studies of land-surface energy balance require temporal and spatial albedo input data without gaps. Several research projects have been devoted to pro-

ducing long-term time series of surface albedo from various satellite-borne sensors (Riihel et al., 2013; Muller et al., 2012; N. F. Liu et al., 2013). However, most of the albedo products do not provide gap-filled time-series albedo maps. Taking the MODIS MCD43B albedo product as an example, 20 to 40 % of the pixels of global landmass miss valid albedo values every year (N. F. Liu et al., 2013). Twenty percent invalid values in albedo input data will result in the same number of empty values in output, an issue that limits the albedo data that can be used in our study. After checking several albedo products (including GlobAlbedo (Muller et al., 2012), CMSAF cClouds, Albedo and Radiation Surface Albedo (CLARA-SAL albedo) (Riihel et al., 2013), and MCD43B), we decided to use GlobAlbedo, as its data do not contain spatial or temporal gaps. This albedo data set is based on a monthly sample, and has a spatial resolution of 0.05° , which we interpolated to a 0.1° resolution for our study.

3.1.4 NDVI

The normalized difference vegetation index (NDVI) is regarded as a reliable indicator of vegetation parameters. NDVI has been used widely to explore vegetation dynamics and their relationships with environmental factors (Piao et al., 2006). NDVI data from the Systeme Pour l'Observation de la Terre (SPOT) VEGETATION sensor, distributed by Vito, have a spatial resolution of $1 \text{ km} \times 1 \text{ km}$ and a temporal resolution of 10 days (synthesized on days 1, 11 and 21 of each month). In order to reduce noise resulting from clouds, the maximum NDVI value in a month for each pixel is selected to represent the canopy status of that month.

3.1.5 Canopy fraction

Canopy fraction (f_c) is defined as the fraction of ground surface covered by the vegetation canopy (varying from 0 to 1). f_c in SEBS is used to distinguish the contributions of vegetation and soil to the roughness parameterization. Here, f_c was

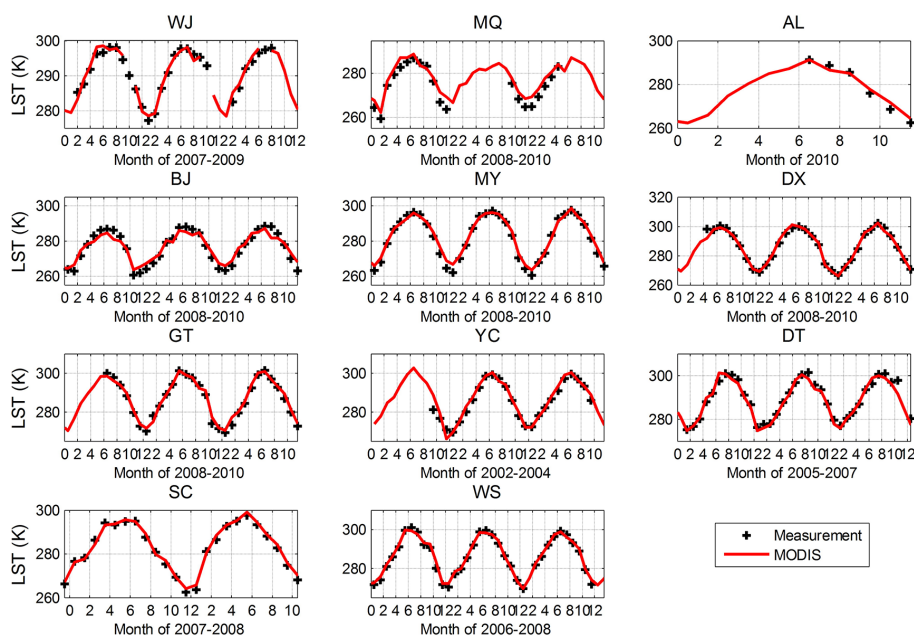


Figure 2. Time-series comparison of monthly averaged LST derived from MOD11C3, MYD11C3 and in situ measurements.

derived from NDVI data using the following equation:

$$f_c = \left[\frac{\text{NDVI} - \min(\text{NDVI}_{\min})}{\max(\text{NDVI}_{\max}) - \min(\text{NDVI}_{\min})} \right]^2 \quad (9)$$

3.2 Validation data

The product generated by our model needed to be validated by comparing it with an independent observational data set. The energy balance measurement system (eddy covariance, four-component radiation and ground heat flux) at flux sites is widely accepted as a method for direct measurement of energy and fluxes, and is widely applied for assessing global evapotranspiration products (Zhang et al., 2010; Jung et al., 2011; Yan et al., 2012; Fisher et al., 2008).

To validate the product, we compiled a data set from 11 flux stations in China with land cover types including bare soil, alpine meadow, cropland, orchard, grassland, and wetlands. The elevations of these stations range from 5 to 4800 m. The observational data set includes data from Maqu (MQ) (Chen et al., 2013b; Wang et al., 2013), Wenjiang (WJ) (Zhang et al., 2012), Bijie (BJ) (Ma et al., 2006), Miyun (MY) (S. M. Liu et al., 2013), Daxing (DX) (S. M. Liu et al., 2013), Guantao (GT) (Liu et al., 2011; S. M. Liu et al., 2013), Yucheng (YC) (Flerchinger et al., 2009), Dongtan (DT) (Zhao et al., 2009), SC (Semi-Arid Climate and Environment Observatory of Lanzhou University) (Huang et al., 2008; Wang et al., 2010; Guan et al., 2009), and Weishan (WS) stations (Lei and Yang, 2010a, b). Detailed information about each site is listed in Table 2.

Half-hourly fluxes were processed using standardized quality control procedures, which are described in the litera-

ture references for each station. The half-hourly H , LE , and four-component radiation was then averaged to monthly values. Monthly average values derived from less than 70 % of the flux data in each month were not used in the validations. Gap filling was not used for the flux measurement data.

4 Results

4.1 Canopy height assessment

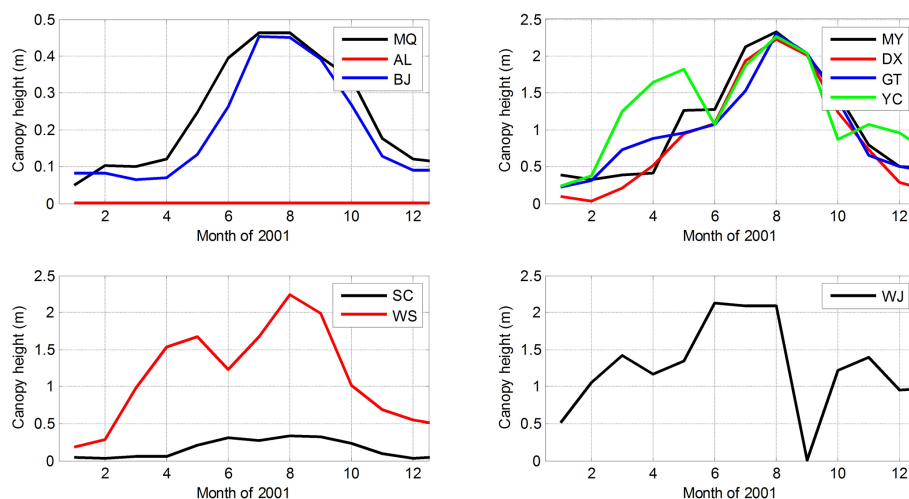
We checked the canopy height variations at the 10 flux stations produced by Eq. (8), and GLAS forest height (Fig. 3). The derived canopy height for AL is about 0, which is reasonable for the local land cover. YC and WS stations, located in northern China, represent typical agricultural land, where crops mature twice per year. The highest canopy height is around 2.2 m, a similar magnitude to the height of maize in summer. The step decrease in canopy height in June at these two stations is due to the fact that wheat/maize is harvested and new seeds are sown during this period. This step variation in the canopy height also causes similar step changes in sensible and latent heat flux (shown by Fig. 5). These canopy height assessments at the observation sites enable us to consider that the developed method in this work is an appropriate one for solving scarcity of canopy height information in a continental area.

4.2 Validation against flux tower measurements

The accuracy of remote-sensing-based land-surface heat fluxes is questionable without validation against ground-

Table 2. Flux tower sites supplying measurement data for product validation.

	Lat (deg) / lon (deg)	Land cover	Eddy covariance	Radiometer	Measurement period	Site elevation (m)	Reference
WJ	30.4200° N/103.5000° E	Crop	CSAT3, Licor7500 (10 HZ)	CNR-1	Mar 2008–Aug 2009	539	Zhang et al. (2012)
MQ	33.8872° N/102.1406° E	Alpine meadow	CSAT3, Licor7500 (10 HZ)	CNR-1	Apr 2009–May 2010	3439	Wang et al. (2013)
AL	33.3905° N/79.7035° E	Bare soil	CSAT3, Licor7500 (10 HZ)	CNR-1	Jul 2010–Dec 2010	4700	Y. Ma et al. (2008)
BJ	31.3686° N/91.8986° E	Alpine grass	CSAT3, Licor7500 (10 HZ)	CNR-1	Jan 2008–Dec 2010	4520	Ma et al. (2011)
MY	40.6038° N/117.323° E	Orchard	CSAT3, Licor7500 (10 HZ)	CNR-1	Jan 2008–Dec 2010	350	S. M. Liu et al. (2013)
DX	39.6213° N/116.4270° E	Crop	CSAT3, Licor7500 (10 HZ)	CNR-1	Jan 2008–Dec 2010	100	S. M. Liu et al. (2013)
GT	36.5150° N/115.1274° E	Crop	CSAT3, Licor7500 (10 HZ)	CNR-1	Jan 2008–Dec 2010	30	S. M. Liu et al. (2013)
YC	36.9500° N/116.600° E	Crop	CSAT3, Licor7500 (10 HZ)	CNR-1	Oct 2002–Oct 2004	13	Flerchinger et al. (2009)
DT	31.5169° N/121.9717° E	Wetland	CSAT3, Licor7500 (10 HZ)	CNR-1	Jan 2005–Dec 2007	5	Zhao et al. (2009)
SC	35.95° N/104.133° E	Dry land	CSAT3, Licor7500 (10 HZ)	CNR-1	Jan 2007–Dec 2008	1965	Huang et al. (2008)
WS	36.6488° N/116.0543° E	Winter wheat/summer maize	CSAT3, Licor7500 (10 HZ)	CNR-1	Jan 2006–Dec 2008	30	Lei and Yang (2010a)

**Figure 3.** Monthly variation of canopy height at the 10 flux stations.

based measurements (Meir and Woodward, 2010). This subsection describes the validation of the SEBS model against heat flux measurements from a diverse range of climates.

In order to analyze the source of flux calculation errors, variables related to surface radiation fluxes were all validated against flux station observations. Table 3 shows that H and LE have RMSE values slightly less than 22 W m^{-2} , which is lower than the RMSE values of products of other statistical methods (see Table 7 in Wang et al., 2007, and Table 5 in Jiménez et al., 2009). Indeed, Kalma et al. (2008) assessed 30 published LE validation results obtained by using ground flux measurements, and reported an average RMSE value of about 50 W m^{-2} and relative errors of 15–30%. The RMSE of our LE data set is significantly lower than their averaged RMSE value.

We also compared our validation results with those of other, similar products produced by a previous version of SEBS. Vinukollu et al. (2011b), for instance, produced global land-surface fluxes with RMSE values of 40.5 W m^{-2} (sensible flux) and 26.1 W m^{-2} (latent flux) (calculated from Table 4 in Vinukollu et al., 2011b), which are larger than those in our study. The difference could be due to the model improvement and more accurate meteorological forcing data

set used in our study. Table 3 lists the values of the statistical parameters for the validation of a data product produced by GLDAS (which has the highest spatial resolution compared with other available terrestrial energy-flux data sets) against the same measurements from the Chinese flux stations as used in our study. According to the mean values of the statistical variables, the quality of our flux data set is comparable to the GLDAS model and data assimilation results. These comparisons of accuracy demonstrate that our revised model is efficient for producing a high-resolution data set of land-surface energy fluxes for China.

Net radiation has relatively higher RMSE and MB values than H , LE and G_0 in the data set, because its accuracy is dependent on the accuracy of the other variable estimates (albedo, LST , SWD , LWD , LWU , etc.). Any errors in these variables can cause bias in net radiation. LWD , for example, has a linear-fitting slope value of 0.9, with most points located around the fitting line (Fig. 4) instead not 1 : 1 line. The correlation coefficient is as high as 0.98, thus demonstrating that there is still room for improvement of the LWD algorithms. LWD in ITPCAS was calculated with algorithms developed from measurements from across the Tibetan Plateau. The LWD algorithms may not, therefore, be

Table 3. Comparison of the accuracy of our flux data product and GLDAS against in situ measurements from 11 Chinese flux towers. MB is the mean of the observation minus the model simulation.

		Energy flux					Radiation flux				
		$H(\text{Wm}^{-2})$	$LE(\text{Wm}^{-2})$	$G_0(\text{Wm}^{-2})$	$R_n(\text{Wm}^{-2})$	Mean	$SWD(\text{Wm}^{-2})$	$SWU(\text{Wm}^{-2})$	$LWD(\text{Wm}^{-2})$	$LWU(\text{Wm}^{-2})$	Mean
Our flux data product	Slope	0.25	1.0	0.87	0.92	0.76	0.95	0.68	0.91	0.95	0.87
	Intercept	0.4	-7.3	6.1	-20.2	-5.1	13.6	10.9	-0.66	16.6	9.9
	RMSE	21.9	21.4	11.7	36.2	22.7	28.3	10.2	32.8	9.6	20.2
	MB	16.0	6.9	-5.7	26.3	11.2	-5.7	-0.65	28.9	2.4	6.2
	R	0.38	0.82	0.50	0.86	0.63	0.89	0.78	0.98	0.99	0.91
	Sample	280	284	197	313	270	310	307	307	307	308
GLDAS	Slope	0.77	0.87	0.58	1.0	0.81	0.99	0.75	0.87	1.0	0.90
	Intercept	20.83	5.1	-1.34	8.0	8.2	34.9	13.1	27.7	-4.5	17.8
	RMSE	26.6	20.6	6.7	17.9	17.9	45.6	15.9	19.2	11.1	23.0
	MB	-15.8	0.75	3.0	-10.4	-5.6	-32.87	-4.6	13.5	-3.2	-6.8
	R	0.46	0.80	0.61	0.95	0.71	0.87	0.65	0.99	0.98	0.87
	Sample	249	250	162	281	236	275	272	272	275	274

Table 4. Comparison of statistical values reported in similar studies.

Reference	Research area	Method	Statistical parameters	$H(\text{Wm}^{-2})$	$LE(\text{Wm}^{-2})$	Flux network	Note
This study	Chinese land-mass	SEBS	RMSE	21.9	21.4	Flux towers in China	
			MB	16.0	6.9		
			R	0.38	0.82		
Wang et al. (2007)	Southern Great Plains, USA	Regression method	RMSE	–	29.8	Flux towers in Southern Great Plains, USA	Calculated from Table 9
			MB	–	12.17		
			R	–	0.91		
Jiménez et al. (2009)	Global	Statistical method	RMSE	–	–	AmeriFlux	Calculated from Tables 5 and 7
			MB	-5.23	7.9		
			R	0.68	0.76		
Vinukollu et al. (2011b)	Global	SEBS	RMSE	40.5	26.1	AmeriFlux	Calculated from Table 4
			MB	27.98	-7.74		
			R	0.53	0.51		

accurate for other parts of China (K. Yang, personal communication, 2013). This underlines the need for more accurate LWD radiation fluxes in order to improve the accuracy of turbulent fluxes and evapotranspiration.

In addition to the statistical evaluation of model results against observations, seasonal and inter-annual changes in the model results also need to be checked. Yucheng station, which is an agricultural experimental station with winter wheat and summer maize as dominant crops, was taken as an example (Fig. 5). Crops at Yucheng station mature twice per year, which is representative of warm temperate farming cropland, typical for the North China Plain. A 2-year flux data set was used to compare against values extracted from our model-derived product. The inter-annual and sea-

sonal LST and LWU data closely match the in situ observations. The SWD term also successfully captures seasonal variations. LWD is systematically lower than observations. The LE produced at Yucheng station not only captures seasonal variation, but also responds at step stages, which occur when the wheat is harvested or maize seeds have just been sown (from June to August). The increased sensible heat and decreased latent heat flux observed in July 2003 were caused by the wheat harvest; however, this signal change is not captured by the model result. The simulated sensible and latent heat produced by SEBS has a 1-month lag when compared to reality. This phenomenon is caused by adopting a maximum monthly NDVI value, resulting in faulty representation of canopy status changes in the month of June.

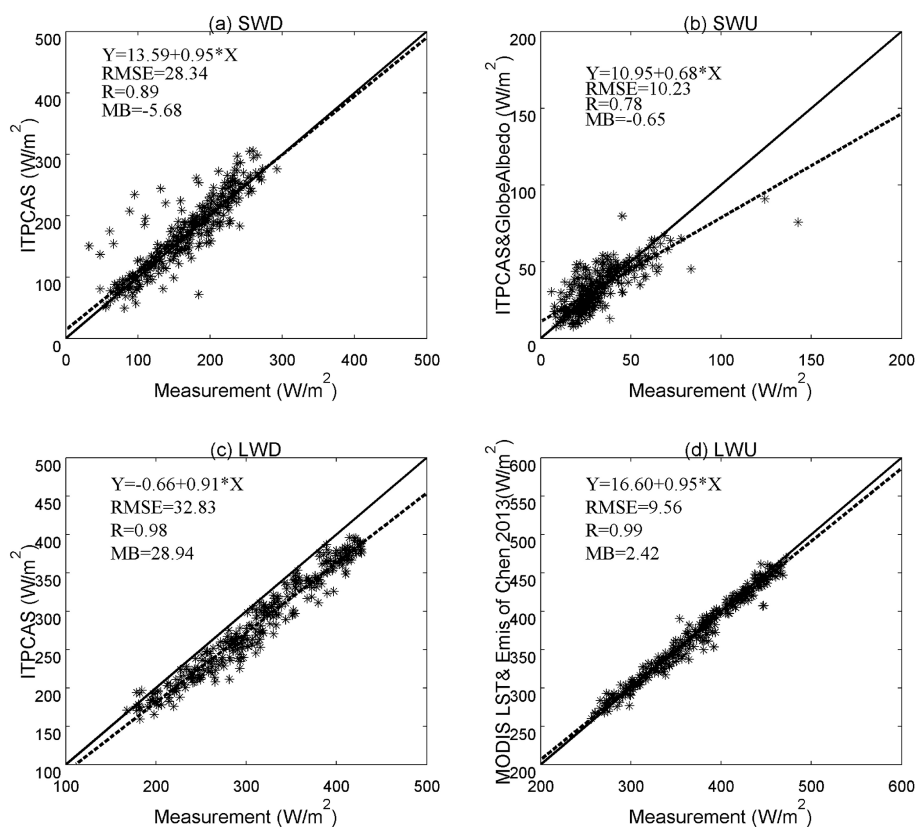


Figure 4. Scatter point for downward short-wave (SWD), upward short-wave (SWU), downward long-wave (LWD), and upward long-wave (LWU) radiation against in situ measurement.

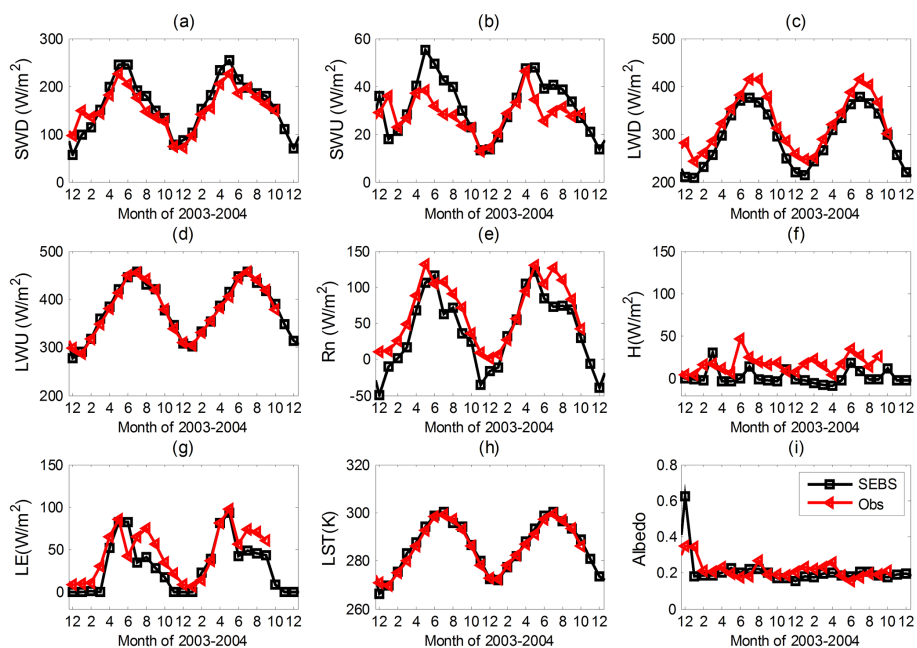


Figure 5. Time-series comparison of SEBS input and output variables against measurements at Yucheng station. Black lines are SEBS results; red lines are measured values.

The Semi-Arid Climate and Environment Observatory of Lanzhou University (SC station) is situated on China's Loess Plateau, at 1965.8 m a.s.l. Annual mean precipitation there is 381.1 mm, and annual evapotranspiration is 1528.5 mm (Huang et al., 2008). Being typical of stations operating under arid conditions, its flux measurements were compared with the grid point values extracted from the model product (Fig. 6). In 2008, the land surface around the station was covered by snow from 19 January to 20 February. Consequently, the GlobAlbedo value was high for February. Unexpectedly, albedo was relatively low for January, which could be caused by the coarse temporal sampling of the station pixel by the satellite sensor. The calculated monthly sensible heat and latent heat in January 2008 have biases of -11.7 (with an observed monthly mean sensible heat of 15 W m^{-2}) and -7.6 W m^{-2} (with an observed monthly mean latent heat of 4.8 W m^{-2}), respectively. The relatively large bias for SC station when covered with snow may be caused by the mixed pixel around the station.

The results of other stations have been included in the Supplement submitted with this paper. Comparison with the results of these other stations shows that model estimates of surface energy balance variables match the magnitude and seasonal variation observed at stations in several contrasting ecosystems. Comparisons between the flux-tower-measured and modeled fluxes show that latent fluxes were more accurate than sensible fluxes. Comparisons with other studies, which are presented in Table 4, show that the accuracy of our data set is one of the best among high-resolution data sets of land-surface fluxes.

4.3 Spatial distribution of land-surface energy fluxes.

Using maps of average annual land-surface radiation and energy fluxes, we analyzed the spatial patterns of radiation and energy fluxes for the Chinese landmass and compared them with other products, such as GLDAS. The highest values of downward surface solar radiation (Fig. 7a) are located in the southwest of the Tibetan Plateau, while the lowest values occur in the Sichuan Basin (SB). The highest levels of upward short-wave radiation (Fig. 7c) occur around the snow-covered peaks of the Himalaya (HM), Karakorum (KRM), Kunlun (KLM), Qilian (QLM) and Nyainqentanglha (NQM) mountain ranges. The strongest net solar radiation (SWD minus SWU) on the Chinese landmass occurs in the southern part of the Tibetan Plateau (see supplementary materials). The downward and upward long-wave radiation (Fig. 7b and c) on the Tibetan Plateau are the lowest for the entire Chinese landmass. Southern China has the highest levels of upward and downward long-wave radiation. The highest values of net long-wave radiation (LWU minus LWD) occur in the southern and western parts of the Tibetan Plateau (see Supplement).

Figure 8 shows that northwestern China (NWC), the western Tibetan Plateau (TP), the inner Mongolian Plateau (MP)

and the Loess Plateau (LP) have the highest yearly average values for surface-sensible heat flux. Croplands of the northern China Plain (NCP, including the lowlands of Shandong, Henan, and Hebei provinces) and the northeastern China Plain (NEP, including the lowlands of Liaoning, Jilin, and Heilongjiang provinces) have low average yearly values for sensible heat flux. The Pearl River delta (PRD) and Tarim (TRB) and Sichuan (SCB) basins also have low levels of sensible heat flux, as do the Yinchuan (YCB) and the inner Mongolian basins (IMB) along the Yellow River. This spatial distribution is consistent with GLDAS results (see Supplement).

Simulated annual latent heat fluxes (Fig. 8b) exhibit a southeast-to-northwest decreasing gradient, which is consistent with other studies (Y. Liu et al., 2013). The southeastern Tibetan Plateau has high levels of annual latent heat flux. The Gobi Desert, in the northwest of China (NWC), has the lowest annual latent heat flux, followed by the western Tibetan Plateau and the inner Mongolian Plateau (MP). Lake regions along the Yangtze River and the region of basins along the Yellow River have relatively high levels of latent heat flux.

The highest levels of annual average surface net radiation (Fig. 8c) can be found in southwestern China and the Lhasa Basin (LB); the lowest levels occur in the Sichuan Basin (SCB) and the Junggar Basin (JB). The highest levels of annual average ground-heat flux (Fig. 8c) are to be found in western China, due to large amounts of incoming solar radiation that occur under dry conditions. The monthly average of G_0 is negligible when compared with other fluxes.

The role of plateau heating in Asia's monsoons is being discussed vigorously (Qiu, 2013; Wu et al., 2012; Boos and Kuang, 2010). Figure 9 shows seasonal comparisons of H between boreal winter (DJF), spring (MAM), summer (JJA) and autumn (SON). The largest area of positive sensible heating occurs in spring. Lee et al. (2011) have shown that contrasting sensible heat fluxes between the Chinese landmass and the seas surrounding it during the pre-monsoon period (April–May) affect monsoon development in East Asia. Figure 9a shows that sources of sensible heating in spring occur over the Tibetan and several other plateaus in China. During summer, the highest sensible heat fluxes are to be found on the western Tibetan Plateau, the eastern Loess Plateau (LP) and in northwestern China (NWC).

LE in summer has the largest area of high latent heating, followed by that in spring, autumn and winter (Fig. 10). Latent heat in summer is highest in southeastern and southern China, as a result of abundant rainfall in these regions. Similarly on irrigated land, such as that found in Yinchuan (YB), the inner Mongolian basin (IMB) and the downstream basins of the Tianshan (TM) and Kunlun (KLM) mountains, latent heat and evapotranspiration are high, due to the ample supply of water in summer. Latent heat fluxes in autumn and winter are significantly lower than those of the other two seasons. The magnitudes and spatial patterns of LE in China of our product are generally consistent with other reports (Yao et al., 2013; Mu et al., 2007; Jung et al., 2010).

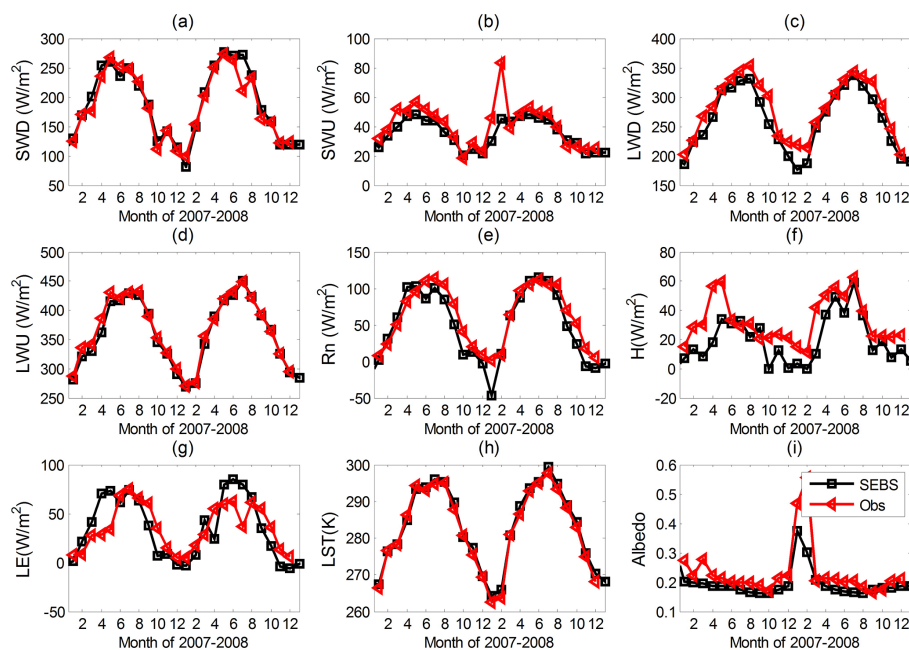


Figure 6. Time-series comparison of SEBS input and output variables against measurements at SC station. Black lines are SEBS results; red lines are measured values.

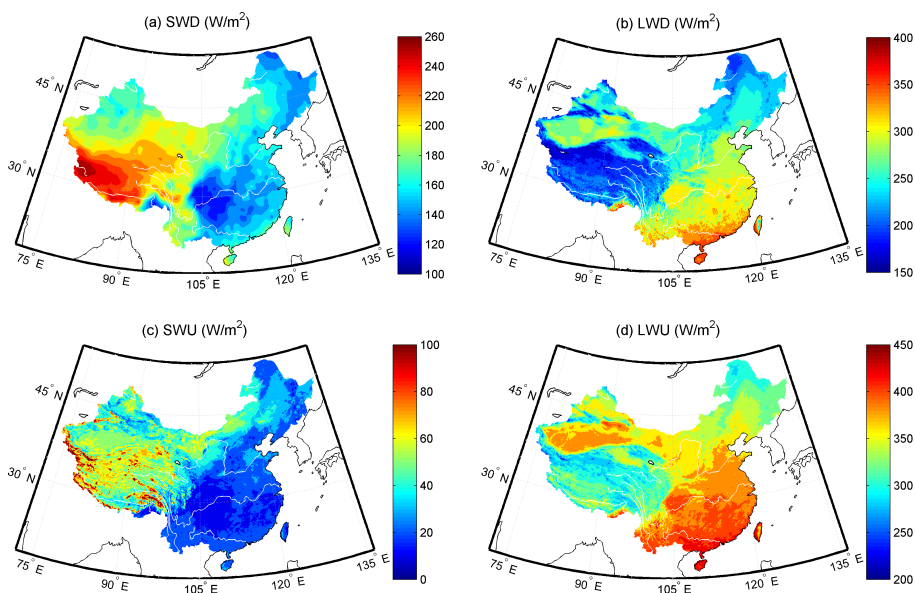


Figure 7. Maps of annual average (a) downward short-wave radiation (SWD), (b) downward long-wave radiation (LWD), (c) upward short-wave radiation (SWU), and (d) upward long-wave radiation (LWU) from 2001 to 2010. Black lines show several major rivers in China.

Net radiation in summer has the highest values of the four seasons. Most of the Chinese landmass acts as a source of surface energy for the atmosphere (Fig. 11).

4.4 Trend analysis

The ability to capture the inter- and intra-annual variation for each land-surface energy variable is of interest to researchers

of monsoon phenomena and climate change (Zhu et al., 2012). Indeed, understanding these variations is essential for studies on climate change and water-resource-related issues. We have calculated annual average values for each flux variable. The nonparametric Mann–Kendall (MK) test is one of the most widely used methods for hydro-meteorological time series analysis (Z. Liu et al., 2013; Gan, 1998). The MK method was applied to the series of annual average fluxes to

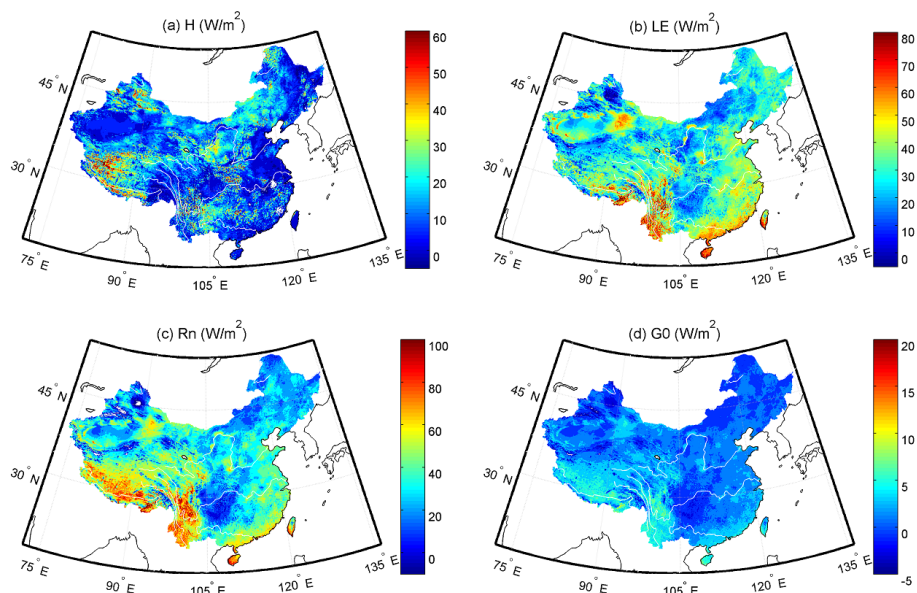


Figure 8. Maps of multiyear (2001–2010) means of retrieved fluxes: **(a)** sensible heat flux (H), **(b)** latent heat flux (LE), **(c)** net radiation (R_n), and **(d)** ground heat flux (G_0). White lines show several major rivers in China.

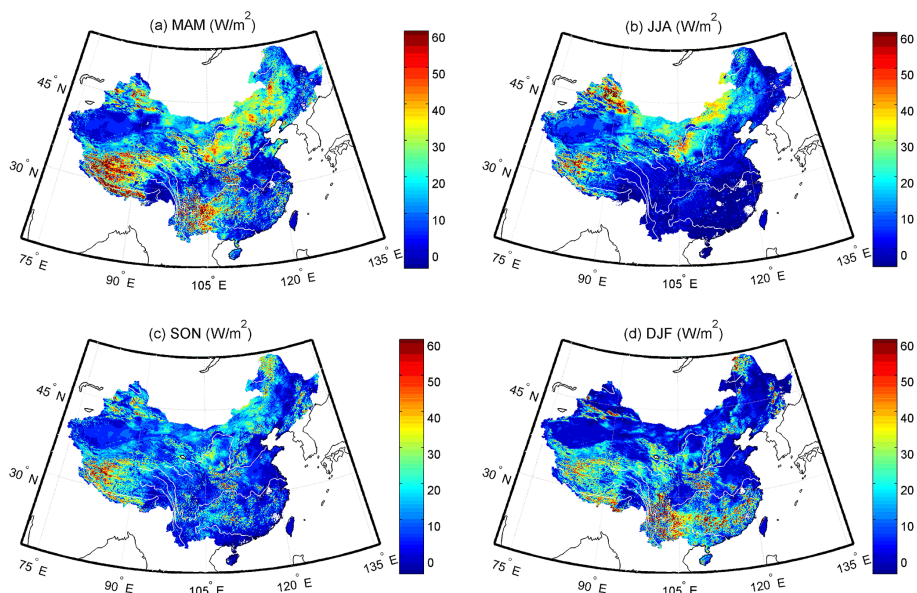


Figure 9. Maps of seasonal average sensible heat flux for **(a)** March–May (MAM), **(b)** June–August (JJA), **(c)** September–November (SON), and **(d)** December–February (DJF) from 2001 to 2010. Black lines show several major rivers in China.

check variations during the period 2001–2010. The resulting slope indicates that downward surface short-wave radiation increased during that decade over the majority of the Tibetan Plateau (Fig. 12).

The ground solar measurements at China Meteorological Administration (CMA) stations from 2003 to 2006, as shown in Fig. 1b of Yang et al. (2012), confirm the increasing trend of downward surface short-wave radiation found in our study. The annual mean visibility measured at these sta-

tions also displays an increasing trend (Fig. 2a of Yang et al., 2012), while ERA-40 reanalyzed precipitable water and station-observed specific humidity show a decreasing trend from 2000 to 2006 (Fig. 3a of Yang et al., 2012). These results indicate that the atmosphere over the plateau is becoming drier, which would explain why SWD has increased during the decade.

The upward short-wave radiation over the Himalaya (HM), Ganges (GM), Karakorum (KRM), Qilian (QLM)

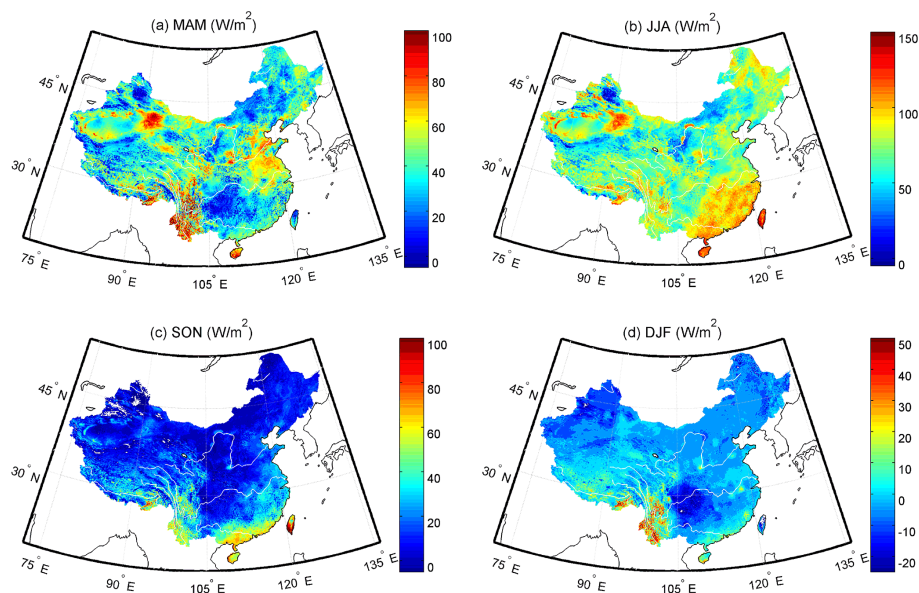


Figure 10. Maps of seasonal average latent heat flux for (a) March–May (MAM), (b) June–August (JJA), (c) September–November (SON), and (d) December–February (DJF) from 2001 to 2010. White lines show several major rivers in China.

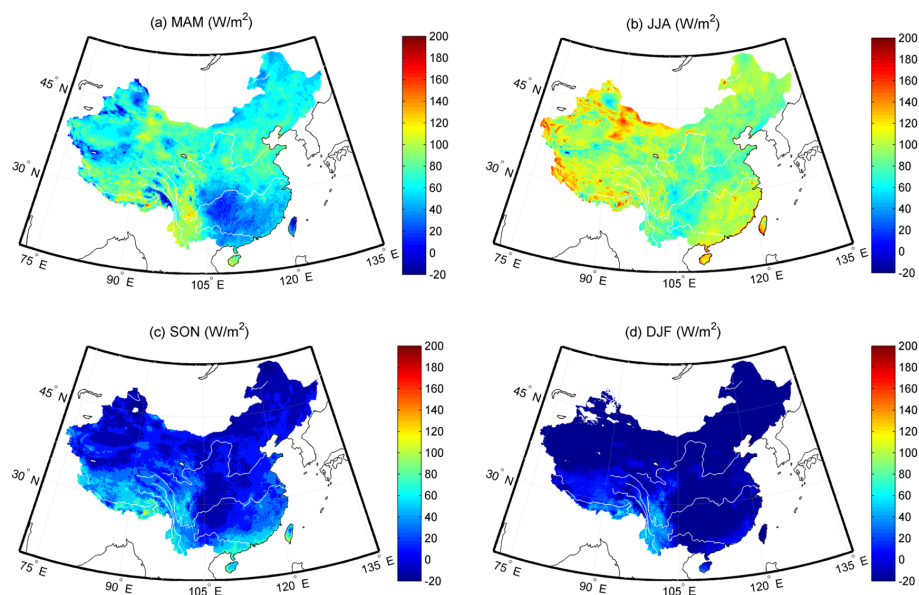


Figure 11. Maps of seasonal average net radiation for (a) March–May (MAM), (b) June–August (JJA), (c) September–November (SON), and (d) December–February (DJF) from 2001 to 2010. White lines show several major rivers in China.

and Nyainqentanglha (NQM) mountain ranges has also decreased over the last 10 years, which may be caused by the glacial retreat that has occurred in these areas (Scherler et al., 2011; Yao et al., 2004). The Lhasa Basin (LB) has the steepest rising trend in LWU, perhaps because of the relatively greater degree of anthropogenic (e.g., urbanization) activity occurring in this area. The trend analysis did not reveal any clear spatial pattern in downward long-wave radiation. Net radiation over several high mountain ranges (including

the Himalaya, Ganges, Karakorum, Qilian and Nyainqentanglha mountain ranges) increased by approximately 5 W m^{-2} between 2001 and 2010 (Fig. 13). The strongest increase in net radiation occurred in the central part of the Tibetan Plateau. As Matthew (2010) has pointed out, soil moisture in the central Tibetan Plateau showed an increasing trend from 1987 to 2008. Wetter soil can cause the ground surface to absorb more net radiation and thus increase latent heat flux. Moreover, wetter soil can increase soil heating capac-

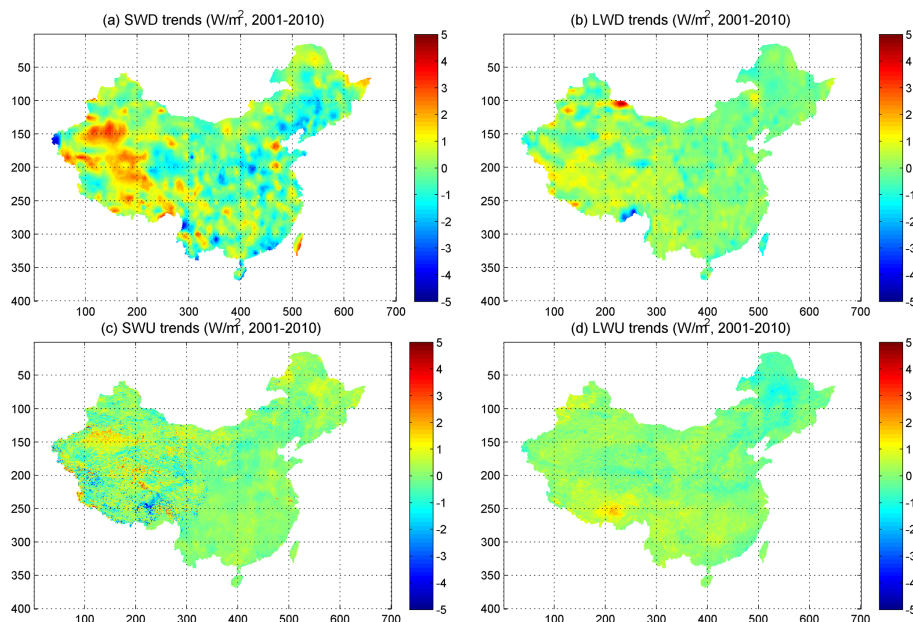


Figure 12. Spatial trends of (a) SWD (downward short-wave), (b) LWD (downward long-wave), (c) SWU (upward short-wave), and (d) LWU (upward long-wave) radiation for the Chinese landmass from 2001 to 2010.

ity (Guan et al., 2009) and so further increase ground heat flux. The increases in net radiation and soil moisture may also explain a rising trend in latent heat in the central Tibetan Plateau. Clearly, the plateau is experiencing accelerated environmental changes (Zhong et al., 2011; Salama et al., 2012). Indeed, land-surface radiation and energy trend analyses also show that the Tibetan Plateau is experiencing a relatively stronger change in land-surface radiation – verified by Tang et al. (2011) – and energy exchange than other parts of China.

5 Conclusions and discussion

In view of China's highly fragmented landscape, high-resolution land-surface heat flux maps are necessary for hydrological studies. As China includes arid, semi-arid, humid, and semi-humid regions, quantifying its water and energy budgets is a challenge. We have developed the surface energy balance system (SEBS) further to produce a land-surface heat flux data set on a continental scale of higher resolution than data sets derived using other methods. Generally, the global surface energy flux data sets, including reanalysis data, do not have enough spatial and temporal resolution when looking at the national-level fluxes. The surface flux data sets from reanalysis data sets still contain large uncertainty, partly due to the deficiency in their land-surface process model that simulates land-surface temperature by solving soil thermal transport equations (Chen et al., 1996), and usually result in a large error in LST simulation (Chen et al., 2011; Wang et al., 2014) if the model is not properly calibrated by measure-

ments (Hogue et al., 2005). Therefore, the hypothesis tested in this paper is whether it is possible to neglect the complex process in the soil by using satellite-observed land-surface temperature directly to calculate the land-surface fluxes on a continental scale. This study has demonstrated a benchmark on how to use satellites to derive a land-surface flux data set for a continental area on a personal laptop, which is absolutely not feasible for the land-surface process modeler to do in such a time- and resource-economic way. We have overcome the shortcomings of previous remotely sensed evapotranspiration products that have null values in barren and desert areas. Usually, the surface roughness length is given a fixed value in numerical models. Here, we also found a solution on how to produce a dynamic surface roughness length due to variations in the canopy height for a continental area. This work will provide suggestions on canopy height to the numerical modelers. In summary, using remote sensing data and surface meteorological information, an independent data product of monthly resolution has been developed for land-surface heat flux analysis. We have validated our remote-sensing-based approach with in situ observations from 11 flux stations in China. Taking into account the limitations of the available spatial data and computing resources, we applied the model to the entire Chinese landmass using a 0.1° resolution meteorological data set, MODIS LST, vegetation indices and other variables to generate a climatological data set of land-surface energy balance for a 10-year period. The modeling results for both pixel-point and spatial distribution demonstrate that this approach meets our aims in terms of (a) being robust across a variety of land cover and climate

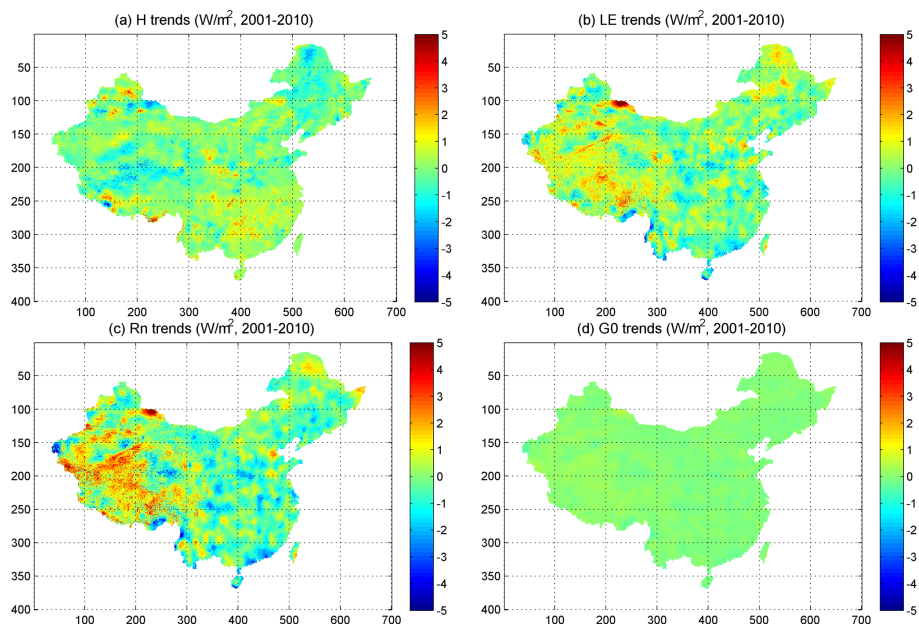


Figure 13. Spatial trends of (a) sensible heat flux (H), (b) latent heat flux (LE), (c) net radiation (R_n), and (d) ground heat flux (G_0) on the Chinese landmass from 2001 to 2010.

types, and (b) performing well for the temporal and spatial scales of interest. The spatial distribution maps generated for each variable of surface energy balance give important background information on the terrestrial hydrology and energy cycles. This product also demonstrates the impact of topography and climatic conditions on land–air energy and moisture exchanges in China.

The applicability of remote-sensing-based estimates of land-surface fluxes is hampered by the limited temporal coverage of satellite sensors (Ryu et al., 2012). Remote sensing data are snapshots of the land-surface status at a particular point in space and time (Ryu et al., 2011). It is challenging to compare remote-sensing-based monthly flux data with ground measurements that are made on timescales ranging from half-hourly through to monthly. The accuracy of land-surface heat fluxes is largely dependent on the remotely sensed land-surface temperature. Here, we have made an assumption that the averaged Aqua and Terra sensor-sensed LST in each month can represent the monthly average LST. The Terra satellite sensor passes twice a day (at about 10:30 a.m. and 22:30 p.m. local time); the Aqua satellite also passes twice a day (at about 01:30 a.m. and 13:30 p.m. local time); so, MODIS has maximally four samples each day. The samples may not be enough for calculating the monthly LST, also due to the cloud noise. Besides, the time length of MODIS data sets is not longer than 15 years, which may limit the application of our data set in climate analysis. Additionally, the sensible heat flux over forest is underestimated by the present turbulent flux parameterization method in SEBS, which does not take the roughness sublayer over high canopy (Bosveld, 1999) into consideration. The low bias in the wind

speed of the ITPCAS forcing data set (not shown here) could also be one reason for the lower estimation of sensible heat flux by our method.

The energy flux product we have developed has a spatial resolution of approximately 10 km, while flux towers have a footprint of tens to hundreds of meters. The tower footprint may not be representative of the larger pixel of the product, and this mismatch will result in errors if the mean of the satellite pixel is different from that of the flux tower footprint. Remote-sensing-based studies stress that direct comparison is a challenge because scale mismatch (Norman et al., 2003) and the heterogeneity of the land surface reduce the spatial representativeness of ground-site measurements (Mi et al., 2006). Another challenge is validating the grid-box-based simulation results on the scale of the Chinese landmass, since reliable observations of flux data are only available from a few sites in the simulated region.

Potential effects of changes in land-surface heat fluxes on the monsoon over East Asia (Lee et al., 2011) as a result of China's recent urbanization can be studied further using our product. As an independent satellite-based product, it can also be used as a data source for evaluating land-surface models. We also produced an evapotranspiration product for the China land area using the data set in this paper. The land-surface fluxes and evapotranspiration product can be downloaded from the URL. The recent product will be shared when the input data set is available: <https://drive.google.com/folderview?id=0B7yGrB1U9eDec2JFbnA5eldlVHc&usp=sharing>.

The Supplement related to this article is available online at doi:10.5194/acp-14-13097-2014-supplement.

Acknowledgements. This work was under the auspices of the Chinese Academy of Sciences (XDB03030201), the National Natural Foundation of China (91337212, 41275010), the CMA Special Fund for Scientific Research in the Public Interest (GYHY201406001), the CAS-KNAW joint PhD project, the CAS-KNAW China Exchange program, the ESA WACMOS project and the FP7 CORE-CLIMAX project. The forcing data set used in our study was developed at the Data Assimilation and Modeling Center for Tibetan Multi-spheres, Institute of Tibetan Plateau Research, Chinese Academy of Sciences. We thank Yang Kun for his comments during the writing of this paper. For our study, we used eddy covariance data acquired from the scientific community and networks. We acknowledge the Wenjiang, Ali, Yucheng, and Weishan stations, the Nagqu Station of Plateau Climate and Environment, the Magqu Zoige Plateau Wetlands Ecosystem Research Station, and the Semi-Arid Climate and Environment Observatory of Lanzhou University for providing their in situ measurement data sets. We also acknowledge Xiangde Xu (CMA), Lide Tian (ITP, CAS), Yu Zhang (CAREERI, CAS), Shouhua Xu (IGSNRR, CAS), Bin Zhao (Fudan University), and Huimin Lei (Tsinghua University) for providing us with their flux data sets. Special thanks to the editor, Nobuko Saigusa.

Edited by: N. Saigusa

References

- Allen, R., Irmak, A., Trezza, R., Hendrickx, J. M. H., Bastiaanssen, W., and Kjaersgaard, J.: Satellite-based ET estimation in agriculture using SEBAL and METRIC, *Hydrol. Process.*, 25, 4011–4027, doi:10.1002/hyp.8408, 2011.
- Boos, W. R. and Kuang, Z.: Dominant control of the South Asian monsoon by orographic insulation versus plateau heating, *Nature*, 463, 218–222, doi:10.1038/nature08707, 2010.
- Bosveld, F. C.: Exchange processes between a coniferous forest and the atmosphere, Ph.D, Wageningen University, 181 pp., 1999.
- Brauman, K., Daily, G., Duarte, T., and Mooney, H.: The nature and value of ecosystem services: An overview highlighting hydrologic services, in: *Annual Review of Environment and Resources*, Annual Review of Environment and Resources, Annu. Rev., Palo Alto, 67–98, 2007.
- Brutsaert, W.: Aspects of bulk atmospheric boundary layer similarity under free-convective conditions, *Rev. Geophys.*, 37, 439–451, doi:10.1029/1999rg900013, 1999.
- Cammalleri, C., Anderson, M. C., Ciruolo, G., D’Urso, G., Kustas, W. P., La Loggia, G., and Minacapilli, M.: The impact of incanopy wind profile formulations on heat flux estimation in an open orchard using the remote sensing-based two-source model, *Hydrol. Earth Syst. Sci.*, 14, 2643–2659, doi:10.5194/hess-14-2643-2010, 2010.
- Chen, F., Mitchell, K., Schaake, J., Xue, Y., Pan, H.-L., Koren, V., Duan, Q. Y., Ek, M., and Betts, A.: Modeling of land surface evaporation by four schemes and comparison with FIFE observations, *J. Geophys. Res.-Atmos.*, 101, 7251–7268, doi:10.1029/95jd02165, 1996.
- Chen, J., Jönsson, P., Tamura, M., Gu, Z., Matsushita, B., and Eklundh, L.: A simple method for reconstructing a high-quality NDVI time-series data set based on the Savitzky–Golay filter, *Remote Sens. Environ.*, 91, 332–344, doi:10.1016/j.rse.2004.03.014, 2004.
- Chen, X., Su, Z., Ma, Y., Yang, K., and Wang, B.: Estimation of surface energy fluxes under complex terrain of Mt. Qomolangma over the Tibetan Plateau, *Hydrol. Earth Syst. Sci.*, 17, 1607–1618, doi:10.5194/hess-17-1607-2013, 2013a.
- Chen, X., Su, Z., Ma, Y., Yang, K., Wen, J., and Zhang, Y.: An Improvement of Roughness Height Parameterization of the Surface Energy Balance System (SEBS) over the Tibetan Plateau, *J. Appl. Meteorol. Clim.*, 52, 607–622, doi:10.1175/jamc-d-12-056.1, 2013b.
- Chen, Y., Yang, K., He, J., Qin, J., Shi, J., Du, J., and He, Q.: Improving land surface temperature modeling for dry land of China, *J. Geophys. Res.*, 116, D20104, doi:10.1029/2011jd015921, 2011.
- Chen, Y., Yang, K., Qin, J., Zhao, L., Tang, W., and Han, M.: Evaluation of AMSR-E retrievals and GLDAS simulations against observations of a soil moisture network on the central Tibetan Plateau, *J. Geophys. Res.-Atmos.*, 118, 4466–4475, doi:10.1002/jgrd.50301, 2013.
- Coll, C., Wan, Z., and Galve, J. M.: Temperature-based and radiance-based validations of the V5 MODIS land surface temperature product, *J. Geophys. Res.*, 114, D20102, doi:10.1029/2009jd012038, 2009.
- Collection-5 MODIS land surface temperature products users’ guide, available at: <http://www.ices.ucsb.edu/modis/LstUsguide/usrguide.html>, 2009.
- Decker, M., Brunke, M. A., Wang, Z., Sakaguchi, K., Zeng, X., and Bosilovich, M. G.: Evaluation of the Reanalysis Products from GSFC, NCEP, and ECMWF Using Flux Tower Observations, *J. Climate*, 25, 1916–1944, doi:10.1175/jcli-d-11-00004.1, 2011.
- Dee, D. P., Uppala, S. M., Simmons, A. J., Berrisford, P., Poli, P., Kobayashi, S., Andrae, U., Balmaseda, M. A., Balsamo, G., Bauer, P., Bechtold, P., Beljaars, A. C. M., van de Berg, L., Bidlot, J., Bormann, N., Delsol, C., Dragani, R., Fuentes, M., Geer, A. J., Haimberger, L., Healy, S. B., Hersbach, H., Hólm, E. V., Isaksen, I., Kållberg, P., Köhler, M., Matricardi, M., McNally, A. P., Monge-Sanz, B. M., Morcrette, J. J., Park, B. K., Peubey, C., de Rosnay, P., Tavolato, C., Thépaut, J. N., and Vitart, F.: The ERA-Interim reanalysis: configuration and performance of the data assimilation system, *Q. J. Roy. Meteor. Soc.*, 137, 553–597, doi:10.1002/qj.828, 2011.
- Dirmeyer, P. A., Gao, X., Zhao, M., Guo, Z., Oki, T., and Hanasaki, N.: GSWP-2: Multimodel Analysis and Implications for Our Perception of the Land Surface, *B. Am. Meteorol. Soc.*, 87, 1381–1397, doi:10.1175/bams-87-10-1381, 2006.
- Fan, L., Liu, S., Bernhofer, C., Liu, H., and Berger, F. H.: Regional land surface energy fluxes by satellite remote sensing in the Upper Xilin River Watershed (Inner Mongolia, China), *Theor. Appl. Climatol.*, 88, 231–245, doi:10.1007/s00704-006-0241-9, 2007.
- Fisher, J. B., Tu, K. P., and Baldocchi, D. D.: Global estimates of the land–atmosphere water flux based on monthly AVHRR and

- ISLSCP-II data, validated at 16 FLUXNET sites, *Remote Sens. Environ.*, 112, 901–919, doi:10.1016/j.rse.2007.06.025, 2008.
- Flerchinger, G., Xaio, W., Marks, D., Sauer, T., and Yu, Q.: Comparison of algorithms for incoming atmospheric long-wave radiation, *Water Resour. Res.*, 45, W03423, doi:10.1029/2008wr007394, 2009.
- Gan, T. Y.: Hydroclimatic trends and possible climatic warming in the Canadian Prairies, *Water Resour. Res.*, 34, 3009–3015, doi:10.1029/98wr01265, 1998.
- Goudriaan, J.: Crop micrometeorology: a simulation study, PhD thesis, Wageningen University 249 pp., 1977.
- Guan, X., Huang, J., Guo, N., Bi, J., and Wang, G.: Variability of soil moisture and its relationship with surface albedo and soil thermal parameters over the Loess Plateau, *Adv. Atmos. Sci.*, 26, 692–700, 2009.
- He, J.: Development of surface meteorological dataset of China with high temporal and spatial resolution, M.S. Inst. of Tibetan Plateau Res., Chin. Acad. of Sci., Beijing, China, 2010.
- Hogue, T. S., Bastidas, L., Gupta, H., Sorooshian, S., Mitchell, K., and Emmerich, W.: Evaluation and Transferability of the Noah Land Surface Model in Semiarid Environments, *J. Hydrometeorol.*, 6, 68–84, doi:10.1175/jhm-402.1, 2005.
- Hsu, H.-H. and Liu, X.: Relationship between the Tibetan Plateau heating and East Asian summer monsoon rainfall, *Geophys. Res. Lett.*, 30, 2066, doi:10.1029/2003gl017909, 2003.
- Huang, J., Zhang, W., Zuo, J., Bi, J., Shi, J., Wang, X., Chang, Z., Huang, Z., Yang, S., Zhang, B., Wang, G., Feng, G., Yuan, J., Zhang, L., Zuo, H., Wang, S., Fu, C., and Jifan, C.: An overview of the semi-arid climate and environment research observatory over the Loess Plateau, *Adv. Atmos. Sci.*, 25, 906–921, 2008.
- Jia, Z., Liu, S., Xu, Z., Chen, Y., and Zhu, M.: Validation of remotely sensed evapotranspiration over the Hai River Basin, China, *J. Geophys. Res.*, 117, D13113, doi:10.1029/2011jd017037, 2012.
- Jiménez, C., Prigent, C., and Aires, F.: Toward an estimation of global land surface heat fluxes from multisatellite observations, *J. Geophys. Res.*, 114, D06305, doi:10.1029/2008jd011392, 2009.
- Jiménez, C., Prigent, C., Mueller, B., Seneviratne, S. I., McCabe, M. F., Wood, E. F., Rossow, W. B., Balsamo, G., Betts, A. K., Dirmeyer, P. A., Fisher, J. B., Jung, M., Kanamitsu, M., Reichle, R. H., Reichstein, M., Rodell, M., Sheffield, J., Tu, K., and Wang, K.: Global intercomparison of 12 land surface heat flux estimates, *J. Geophys. Res.*, 116, D02102, doi:10.1029/2010jd014545, 2011.
- Jung, M., Reichstein, M., and Bondeau, A.: Towards global empirical upscaling of FLUXNET eddy covariance observations: validation of a model tree ensemble approach using a biosphere model, *Biogeosciences*, 6, 2001–2013, doi:10.5194/bg-6-2001-2009, 2009.
- Jung, M., Reichstein, M., Ciais, P., Seneviratne, S. I., Sheffield, J., Goulden, M. L., Bonal, G., Cescatti, A., Chen, J., de Jeu, R., Dolman, A. J., Eugster, W., Gerten, D., Gianelle, D., Gobron, N., Heinke, J., Kimball, J., Law, B. E., Montagnani, L., Mu, Q., Mueller, B., Oleson, K., Papale, D., Richardson, A. D., Rouspard, O., Running, S., Tomelleri, E., Viovy, N., Weber, U., Williams, C., Wood, E., Zaehle, S., and Zhang, K.: Recent decline in the global land evapotranspiration trend due to limited moisture supply, *Nature*, 467, 951–954, 2010.
- Jung, M., Reichstein, M., Margolis, H. A., Cescatti, A., Richardson, A. D., Arain, M. A., Arneth, A., Bernhofer, C., Bonal, D., Chen, J., Gianelle, D., Gobron, N., Kiely, G., Kutsch, W., Lasslop, G., Law, B. E., Lindroth, A., Merbold, L., Montagnani, L., Moors, E. J., Papale, D., Sottocornola, M., Vaccari, F., and Williams, C.: Global patterns of land-atmosphere fluxes of carbon dioxide, latent heat, and sensible heat derived from eddy covariance, satellite, and meteorological observations, *J. Geophys. Res.*, 116, G00J07, doi:10.1029/2010jg001566, 2011.
- Kalma, J., McVicar, T., and McCabe, M.: Estimating land surface evaporation: a review of methods using remotely sensed surface temperature data, *Surv. Geophys.*, 29, 421–469, doi:10.1007/s10712-008-9037-z, 2008.
- Kalnay, E., Kanamitsu, M., Kistler, R., Collins, W., Deaven, D., Gandin, L., Iredell, M., Saha, S., White, G., Woollen, J., Zhu, Y., Leetmaa, A., Reynolds, R., Chelliah, M., Ebisuzaki, W., Higgins, W., Janowiak, J., Mo, K. C., Ropelewski, C., Wang, J., Jenne, R., and Joseph, D.: The NCEP/NCAR 40-year reanalysis project, *B. Am. Meteorol. Soc.*, 77, 437–471, doi:10.1175/1520-0477(1996)077<0437:tnyrp>2.0.co;2, 1996.
- Lee, E., Barford, C., Kucharik, C., Felzer, B., and Foley, J.: Role of turbulent heat fluxes over land in the monsoon over East Asia, *Int. J. Geosci.*, 2, 420–431, 10.4236/ijg.2011.24046, 2011.
- Lei, H. and Yang, D.: Interannual and seasonal variability in evapotranspiration and energy partitioning over an irrigated cropland in the North China Plain, *Agr. Forest Meteorol.*, 150, 581–589, doi:10.1016/j.agrformet.2010.01.022, 2010a.
- Lei, H. and Yang, D.: Seasonal and interannual variations in carbon dioxide exchange over a cropland in the North China Plain, *Glob. Change Biol.*, 16, 2944–2957, doi:10.1111/j.1365-2486.2009.02136.x, 2010b.
- Li, X., Li, X., Li, Z., Ma, M., Wang, J., Xiao, Q., Liu, Q., Che, T., Chen, E., Yan, G., Hu, Z., Zhang, L., Chu, R., Su, P., Liu, Q., Liu, S., Wang, J., Niu, Z., Chen, Y., Jin, R., Wang, W., Ran, Y., Xin, X., and Ren, H.: Watershed Allied Telemetry Experimental Research, *J. Geophys. Res.-Atmos.*, 114, D22103, doi:10.1029/2008jd011590, 2009.
- Li, X., Liang, S., Yuan, W., Yu, G., Cheng, X., Chen, Y., Zhao, T., Feng, J., Ma, Z., Ma, M., Liu, S., Chen, J., Shao, C., Li, S., Zhang, X., Zhang, Z., Sun, G., Chen, S., Ohta, T., Varlagin, A., Miyata, A., Takagi, K., Saiqusa, N., and Kato, T.: Estimation of evapotranspiration over the terrestrial ecosystems in China, *Ecohydrology*, 7, 139–149, doi:10.1002/eco.1341, 2012.
- Li, X., Wang, L., Chen, D., Yang, K., Xue, B., and Sun, L.: Near-surface air temperature lapse rates in the mainland China during 1962–2011, *J. Geophys. Res.-Atmos.*, 118, 7505–7515, doi:10.1002/jgrd.50553, 2013.
- Li, Z., Zheng, F.-L., and Liu, W.-Z.: Spatiotemporal characteristics of reference evapotranspiration during 1961–2009 and its projected changes during 2011–2099 on the Loess Plateau of China, *Agr. Forest Meteorol.*, 154–155, 147–155, doi:10.1016/j.agrformet.2011.10.019, 2012.
- Lin, W., Zhang, L., Du, D., Yang, L., Lin, H., Zhang, Y., and Li, J.: Quantification of land use/land cover changes in Pearl River Delta and its impact on regional climate in summer using numerical modeling, *Reg. Environ. Change*, 9, 75–82, doi:10.1007/s10113-008-0057-5, 2009.
- Liu, J.-G. and Xie, Z.-H.: Improving simulation of soil moisture in China using a multiple meteorological forcing en-

- semble approach, *Hydrol. Earth Syst. Sci.*, 17, 3355–3369, doi:10.5194/hess-17-3355-2013, 2013.
- Liu, N. F., Liu, Q., Wang, L. Z., Liang, S. L., Wen, J. G., Qu, Y., and Liu, S. H.: A statistics-based temporal filter algorithm to map spatiotemporally continuous shortwave albedo from MODIS data, *Hydrol. Earth Syst. Sci.*, 17, 2121–2129, doi:10.5194/hess-17-2121-2013, 2013.
- Liu, R., Wen, J., Wang, X., Wang, L., Tian, H., Zhang, T. T., Shi, X. K., Zhang, J. H., and Lv, S. N.: Actual daily evapotranspiration estimated from MERIS and AATSR data over the Chinese Loess Plateau, *Hydrol. Earth Syst. Sci.*, 14, 47–58, doi:10.5194/hess-14-47-2010, 2010.
- Liu, S. M., Xu, Z. W., Wang, W. Z., Jia, Z. Z., Zhu, M. J., Bai, J., and Wang, J. M.: A comparison of eddy-covariance and large aperture scintillometer measurements with respect to the energy balance closure problem, *Hydrol. Earth Syst. Sci.*, 15, 1291–1306, doi:10.5194/hess-15-1291-2011, 2011.
- Liu, S. M., Xu, Z. W., Zhu, Z. L., Jia, Z. Z., and Zhu, M. J.: Measurements of evapotranspiration from eddy-covariance systems and large aperture scintillometers in the Hai River Basin, China, *J. Hydrol.*, 487, 24–38, doi:10.1016/j.jhydrol.2013.02.025, 2013.
- Liu, Y., Zhou, Y., Ju, W., Chen, J., Wang, S., He, H., Wang, H., Guan, D., Zhao, F., Li, Y., and Hao, Y.: Evapotranspiration and water yield over China's landmass from 2000 to 2010, *Hydrol. Earth Syst. Sci.*, 17, 4957–4980, doi:10.5194/hess-17-4957-2013, 2013.
- Liu, Z., Zhou, P., Zhang, F., Liu, X., and Chen, G.: Spatiotemporal characteristics of dryness/wetness conditions across Qinghai Province, Northwest China, *Agr. Forest Meteorol.*, 182–183, doi:10.1016/j.agrformet.2013.05.013, 2013.
- Ma, L., Zhang, T., Li, Q., Frauenfeld, O. W., and Qin, D.: Evaluation of ERA-40, NCEP-1, and NCEP-2 reanalysis air temperatures with ground-based measurements in China, *J. Geophys. Res.*, 113, D15115, doi:10.1029/2007jd009549, 2008.
- Ma, Y., Su, Z., Li, Z., Koike, T., and Menenti, M.: Determination of regional net radiation and soil heat flux over a heterogeneous landscape of the Tibetan Plateau, *Hydrol. Process.*, 16, 2963–2971, 2002.
- Ma, Y., Zhong, L., Su, Z., Ishikawa, H., Menenti, M., and Koike, T.: Determination of regional distributions and seasonal variations of land surface heat fluxes from Landsat-7 Enhanced Thematic Mapper data over the central Tibetan Plateau area, *J. Geophys. Res.*, 111, D10305, doi:10.1029/2005jd006742, 2006.
- Ma, Y., Zhong, L., Wang, B., Ma, W., Chen, X., and Li, M.: Determination of land surface heat fluxes over heterogeneous landscape of the Tibetan Plateau by using the MODIS and in situ data, *Atmos. Chem. Phys.*, 11, 10461–10469, doi:10.5194/acp-11-10461-2011, 2011.
- Ma, Y., Kang, S., Zhu, L., Xu, B., Tian, L., and Yao, T.: Tibetan Observation and Research Platform- Atmosphere–land interaction over a heterogeneous landscape, *B. Am. Meteorol. Soc.*, 89, 1487–1492, doi:10.1175/2008BAMS2545.1, 2008.
- Massman, W. J.: An analytical one-dimensional second-order closure model of turbulence statistics and the lagrangian time scale within and above plant canopies of arbitrary structure, *Bound.-Lay. Meteorol.*, 83, 407–421, 1997.
- Matthew, O.: Characterization of the effects of climate variation on land surface temperature and soil moisture through stochastic analysis of long term SSM/I observations over the Tibetan plateau, Master, International Institute for Geo-information Science and Earth Observation, University of Twente, Enschede, the Netherlands, 1–67 pp., 2010.
- Meir, P. and Woodward, F. I.: Amazonian rain forests and drought: response and vulnerability, *New Phytol.*, 187, 553–557, doi:10.1111/j.1469-8137.2010.03390.x, 2010.
- Mi, N., Yu, G. R., Wang, P. X., Wen, X. F., and Sun, X. M.: A preliminary study for spatial representiveness of flux observation at ChinaFLUX sites, *Sci. China Ser. D*, 49, 24–35, 2006.
- Moody, E. G., King, M. D., Platnick, S., Schaaf, C. B., and Feng, G.: Spatially complete global spectral surface albedos: value-added datasets derived from Terra MODIS land products, *IEEE T. Geosci. Remote*, 43, 144–158, doi:10.1109/tgrs.2004.838359, 2005.
- Mu, Q., Heinsch, F. A., Zhao, M., and Running, S. W.: Development of a global evapotranspiration algorithm based on MODIS and global meteorology data, *Remote Sens. Environ.*, 111, 519–536, doi:10.1016/j.rse.2007.04.015, 2007.
- Mueller, B., Seneviratne, S. I., Jimenez, C., Corti, T., Hirschi, M., Balsamo, G., Ciais, P., Dirmeyer, P., Fisher, J. B., Guo, Z., Jung, M., Maignan, F., McCabe, M. F., Reichle, R., Reichstein, M., Rodell, M., Sheffield, J., Teuling, A. J., Wang, K., Wood, E. F., and Zhang, Y.: Evaluation of global observations-based evapotranspiration datasets and IPCC AR4 simulations, *Geophys. Res. Lett.*, 38, L06402, doi:10.1029/2010gl046230, 2011.
- Muller, J.-P., López, G., Watson, G., Shane, N., Kennedy, T., Yuen, P., Lewis, P., Fischer, J., Guanter, L., Domench, C., Preusker, R., North, P., Heckel, A., Danne, O., and Krämer, U.: The ESA Global Albedo Project for mapping the Earth's land surface albedo for 15 Years from European Sensors, *IEEE Geoscience and Remote Sensing Symposium (IGARSS)*, IEEE, Munich, Germany, 2012.
- Norman, J. M., Anderson, M. C., Kustas, W. P., French, A. N., Mecikalski, J., Torn, R., Diak, G. R., Schmugge, T. J., and Tanner, B. C. W.: Remote sensing of surface energy fluxes at 101-m pixel resolutions, *Water Resour. Res.*, 39, 1221, doi:10.1029/2002wr001775, 2003.
- Piao, S., Mohammat, A., Fang, J., Cai, Q., and Feng, J.: NDVI-based increase in growth of temperate grasslands and its responses to climate changes in China, *Glob. Environ. Change*, 16, 340–348, doi:10.1016/j.gloenvcha.2006.02.002, 2006.
- Qiu, J.: Monsoon Melee, *Science*, 340, 1400–1401, doi:10.1126/science.340.6139.1400, 2013.
- Rienecker, M. M., Suarez, M. J., Gelaro, R., Todling, R., Bacmeister, J., Liu, E., Bosilovich, M. G., Schubert, S. D., Takacs, L., Kim, G.-K., Bloom, S., Chen, J., Collins, D., Conaty, A., da Silva, A., Gu, W., Joiner, J., Koster, R. D., Lucchesi, R., Molod, A., Owens, T., Pawson, S., Pegion, P., Redder, C. R., Reichle, R., Robertson, F. R., Ruddick, A. G., Sienkiewicz, M., and Woollen, J.: MERRA: NASA's Modern-Era Retrospective Analysis for Research and Applications, *J. Climate*, 24, 3624–3648, doi:10.1175/jcli-d-11-00015.1, 2011.
- Riihelä, A., Manninen, T., Laine, V., Andersson, K., and Kaspar, F.: CLARA-SAL: a global 28 yr timeseries of Earth's black-sky surface albedo, *Atmos. Chem. Phys.*, 13, 3743–3762, doi:10.5194/acp-13-3743-2013, 2013.
- Roads, J. and Betts, A.: NCEP–NCAR and ECMWF reanalysis surface water and energy budgets for the Mississippi River Basin, *J. Hydrometeorol.*, 1, 88–94, doi:10.1175/1525-7541(2000)001<0088:nnaers>2.0.co;2, 2000.

- Rodell, M., Houser, P. R., Jambor, U., Gottschalck, J., Mitchell, K., Meng, C. J., Arsenault, K., Cosgrove, B., Radakovich, J., Bosilovich, M., Entin, J. K., Walker, J. P., Lohmann, D., and Toll, D.: The Global Land Data Assimilation System, *B. Am. Meteorol. Soc.*, 85, 381–394, doi:10.1175/bams-85-3-381, 2004.
- Ryu, Y., Baldocchi, D. D., Kobayashi, H., van Ingen, C., Li, J., Black, T. A., Beringer, J., van Gorsel, E., Knohl, A., Law, B. E., and Rouspard, O.: Integration of MODIS land and atmosphere products with a coupled-process model to estimate gross primary productivity and evapotranspiration from 1 km to global scales, *Global Biogeochem. Cy.*, 25, GB4017, doi:10.1029/2011gb004053, 2011.
- Ryu, Y., Baldocchi, D. D., Black, T. A., Detto, M., Law, B. E., Leuning, R., Miyata, A., Reichstein, M., Vargas, R., Ammann, C., Beringer, J., Flanagan, L. B., Gu, L., Hutley, L. B., Kim, J., McCaughey, H., Moors, E. J., Rambal, S., and Vesala, T.: On the temporal upscaling of evapotranspiration from instantaneous remote sensing measurements to 8-day mean daily-sums, *Agr. Forest Meteorol.*, 152, 212–222, 2012.
- Salama, M. S., Velde, R., Zhong, L., Ma, Y., Ofwono, M., and Su, Z.: Decadal variations of land surface temperature anomalies observed over the Tibetan Plateau by the Special Sensor Microwave Imager (SSM/I) from 1987 to 2008, *Clim. Change*, 114, 769–781, doi:10.1007/s10584-012-0427-3, 2012.
- Scherler, D., Bookhagen, B., and Strecker, M. R.: Spatially variable response of Himalayan glaciers to climate change affected by debris cover, *Nat. Geosci.*, 4, 156–159, 2011.
- Sheffield, J., Goteti, G., and Wood, E. F.: Development of a 50-Year high-resolution global dataset of meteorological forcings for land surface modeling, *J. Climate*, 19, 3088–3111, doi:10.1175/jcli3790.1, 2006.
- Shu, Y., Stisen, S., Jensen, K. H., and Sandholt, I.: Estimation of regional evapotranspiration over the North China Plain using geostationary satellite data, *Int. J. Appl. Earth Obs.*, 13, 192–206, doi:10.1016/j.jag.2010.11.002, 2011.
- Simard, M., Pinto, N., Fisher, J. B., and Baccini, A.: Mapping forest canopy height globally with spaceborne lidar, *J. Geophys. Res.*, 116, G04021, doi:10.1029/2011jg001708, 2011.
- Su, Z., Schmugge, T., Kustas, W. P., and Massman, W. J.: An evaluation of two models for estimation of the roughness height for heat transfer between the land surface and the atmosphere, *J. Appl. Meteorol.*, 40, 1933–1951, doi:10.1175/1520-0450(2001)040<1933:AEOTMF>2.0.CO;2, 2001.
- Su, Z.: The Surface Energy Balance System (SEBS) for estimation of turbulent heat fluxes, *Hydrol. Earth Syst. Sci.*, 6, 85–100, doi:10.5194/hess-6-85-2002, 2002.
- Su, Z., de Rosnay, P., Wen, J., Wang, L., and Zeng, Y.: Evaluation of ECMWF's soil moisture analyses using observations on the Tibetan Plateau, *J. Geophys. Res.-Atmos.*, 118, 5304–5318, doi:10.1002/jgrd.50468, 2013.
- Suh, M.-S. and Lee, D.-K.: Impacts of land use/cover changes on surface climate over east Asia for extreme climate cases using RegCM2, *J. Geophys. Res.-Atmos.*, 109, D02108, doi:10.1029/2003jd003681, 2004.
- Sun, L. and Wu, G.: Influence of land evapotranspiration on climate variations, *Sci. China Ser. D*, 44, 838–846, doi:10.1007/bf02907096, 2001.
- Tang, W.-J., Yang, K., Qin, J., Cheng, C. C. K., and He, J.: Solar radiation trend across China in recent decades: a revisit with quality-controlled data, *Atmos. Chem. Phys.*, 11, 393–406, doi:10.5194/acp-11-393-2011, 2011.
- Taniguchi, K. and Koike, T.: Seasonal variation of cloud activity and atmospheric profiles over the eastern part of the Tibetan Plateau, *J. Geophys. Res.-Atmos.*, 113, 10104–10104, 2008.
- Timmermans, J.: Coupling optical and thermal directional radiative transfer to biophysical processes in vegetated canopies, Phd, faculty of geo-information science and earth observation, University of Twente, Enschede, the Netherlands, 1–157 pp., 2011.
- Vinukollu, R. K., Meynadier, R., Sheffield, J., and Wood, E. F.: Multi-model, multi-sensor estimates of global evapotranspiration: climatology, uncertainties and trends, *Hydrol. Process.*, 25, 3993–4010, doi:10.1002/hyp.8393, 2011a.
- Vinukollu, R. K., Wood, E. F., Ferguson, C. R., and Fisher, J. B.: Global estimates of evapotranspiration for climate studies using multi-sensor remote sensing data: Evaluation of three process-based approaches, *Remote Sens. Environ.*, 115, 801–823, doi:10.1016/j.rse.2010.11.006, 2011b.
- Wan, Z. and Li, Z. L.: Radiance – validation of the V5 MODIS land – temperature product, *Int. J. Remote Sens.*, 29, 5373–5395, doi:10.1080/0143160802036565, 2008.
- Wan, Z.: Collection-5 MODIS land surface temperature products users' guide, available at: <http://www.ices.ucs.edu/modis/LstUsrGuide/usrguide.html> (last access: 3 December 2014), 2009.
- Wang, A. and Zeng, X.: Evaluation of multireanalysis products with in situ observations over the Tibetan Plateau, *J. Geophys. Res.*, 117, D05102, doi:10.1029/2011jd016553, 2012.
- Wang, A., Barlage, M., Zeng, X., and Draper, C. S.: Comparison of land skin temperature from a land model, remote sensing, and in-situ measurement, *J. Geophys. Res.-Atmos.*, 119, 3093–3106, doi:10.1002/2013jd021026, 2014.
- Wang, G., Huang, J., Guo, W., Zuo, J., Wang, J., Bi, J., Huang, Z., and Shi, J.: Observation analysis of land-atmosphere interactions over the Loess Plateau of northwest China, *J. Geophys. Res.*, 115, D00K17, doi:10.1029/2009jd013372, 2010.
- Wang, K. and Liang, S.: An improved method for estimating global evapotranspiration based on satellite determination of surface net radiation, vegetation index, temperature, and soil moisture, *J. Hydrometeorol.*, 9, 712–727, doi:10.1175/2007jhm911.1, 2008.
- Wang, K., Wang, P., Li, Z., Cribb, M., and Sparrow, M.: A simple method to estimate actual evapotranspiration from a combination of net radiation, vegetation index, and temperature, *J. Geophys. Res.-Atmos.*, 112, D15107, doi:10.1029/2006jd008351, 2007.
- Wang, S., Zhang, Y., Lv, S., Liu, H., and Shang, L.: Estimation of turbulent fluxes using the flux-variance method over alpine meadows surface in eastern Tibetan Plateau, *Adv. Atmos. Sci.*, 30, 411–424, doi:10.1007/s00376-012-2056-1, 2013.
- Wu, G., Liu, Y., He, B., Bao, Q., Duan, A., and Jin, F.-F.: Thermal controls on the Asian summer monsoon, *Sci. Rep.*, 2, 1–7, doi:10.1038/srep00404, 2012.
- Yan, H., Wang, S. Q., Billesbach, D., Oechel, W., Zhang, J. H., Meyers, T., Martin, T. A., Matamala, R., Baldocchi, D., Bohrer, G., Dragoni, D., and Scott, R.: Global estimation of evapotranspiration using a leaf area index-based surface energy and water balance model, *Remote Sens. Environ.*, 124, 581–595, doi:10.1016/j.rse.2012.06.004, 2012.
- Yang, K., Koike, T., Fujii, H., Tamagawa, K., and Hirose, N.: Improvement of surface flux parametrizations with a turbulence-

- related length, *Q. J. Roy. Meteor. Soc.*, 128, 2073–2087, doi:10.1256/003590002320603548, 2002.
- Yang, K., Ding, B., Qin, J., Tang, W., Lu, N., and Lin, C.: Can aerosol loading explain the solar dimming over the Tibetan Plateau?, *Geophys. Res. Lett.*, 39, L20710, doi:10.1029/2012gl053733, 2012.
- Yao, T., Wang, Y., Liu, S., Pu, J., Shen, Y., and Lu, A.: Recent glacial retreat in High Asia in China and its impact on water resource in Northwest China, *Sci. China Ser. D*, 47, 1065–1075, doi:10.1360/03yd0256, 2004.
- Yao, Y., Liang, S., Cheng, J., Liu, S., Fisher, J. B., Zhang, X., Jia, K., Zhao, X., Qin, Q., Zhao, B., Han, S., Zhou, G., Zhou, G., Li, Y., and Zhao, S.: MODIS-driven estimation of terrestrial latent heat flux in China based on a modified Priestley–Taylor algorithm, *Agr. Forest Meteorol.*, 171–172, 187–202, 2013.
- Yu, G.-R., Wen, X.-F., Sun, X.-M., Tanner, B. D., Lee, X., and Chen, J.-Y.: Overview of ChinaFLUX and evaluation of its eddy covariance measurement, *Agr. Forest Meteorol.*, 137, 125–137, doi:10.1016/j.agrformet.2006.02.011, 2006.
- Yuan, W., Liu, S., Yu, G., Bonnefond, J.-M., Chen, J., Davis, K., Desai, A. R., Goldstein, A. H., Gianelle, D., Rossi, F., Suyker, A. E., and Verma, S. B.: Global estimates of evapotranspiration and gross primary production based on MODIS and global meteorology data, *Remote Sens. Environ.*, 114, 1416–1431, doi:10.1016/j.rse.2010.01.022, 2010.
- Zhang, C., Chen, F., Miao, S., Li, Q., Xia, X., and Xuan, C.: Impacts of urban expansion and future green planting on summer precipitation in the Beijing metropolitan area, *J. Geophys. Res.-Atmos.*, 114, D02116, doi:10.1029/2008jd010328, 2009.
- Zhang, K., Kimball, J. S., Nemani, R. R., and Running, S. W.: A continuous satellite-derived global record of land surface evapotranspiration from 1983 to 2006, *Water Resour. Res.*, 46, W09522, doi:10.1029/2009wr008800, 2010.
- Zhang, L., Li, Y., Li, Y., and Zhao, X.: Seasonal changes of turbulent fluxes at a typical agricultural site in the Chengdu Plain based on quality-controlled data, *J. Meteorol. Soc. Jpn.*, 90C, 195–202, 2012.
- Zhang, X., Ren, Y., Yin, Z.-Y., Lin, Z., and Zheng, D.: Spatial and temporal variation patterns of reference evapotranspiration across the Qinghai-Tibetan Plateau during 1971–2004, *J. Geophys. Res.*, 114, D15105, doi:10.1029/2009jd011753, 2009.
- Zhao, B., Yan, Y., Guo, H., He, M., Gu, Y., and Li, B.: Monitoring rapid vegetation succession in estuarine wetland using time series MODIS-based indicators: An application in the Yangtze River Delta area, *Ecol. Indic.*, 9, 346–356, doi:10.1016/j.ecolind.2008.05.009, 2009.
- Zhong, L., Su, Z., Ma, Y., Salama, M. S., and Sobrino, J. A.: Accelerated changes of environmental conditions on the Tibetan Plateau caused by climate change, *J. Climate*, 24, 6540–6550, doi:10.1175/jcli-d-10-05000.1, 2011.
- Zhou, L. and Huang, R.: Interdecadal variability of sensible heat flux in arid and semi-arid region of Northwest China and its relationship to summer precipitation in China (in Chinese), *Chinese J. Atmos. Sci.*, 32, 1276–1288, 2008.
- Zhou, L. and Huang, R.: An assessment of the quality of surface sensible heat flux derived from reanalysis data through comparison with station observations in Northwest China, *Adv. Atmos. Sci.*, 27, 500–512, doi:10.1007/s00376-009-9081-8, 2010.
- Zhu, X., Liu, Y., and Wu, G.: An assessment of summer sensible heat flux on the Tibetan Plateau from eight data sets, *Science China Earth Sciences*, 55, 779–786, doi:10.1007/s11430-012-4379-2, 2012.